universität wien

MASTERARBEIT / MASTER'S THESIS

Titel der Masterarbeit / Title of the Master's Thesis

„Ultrastructural and proteomic alterations induced by hypoxic and shear stress in human ovarian cancer cells"

verfasst von / submitted by

Michelle Kriz, BSc

angestrebter akademischer Grad / in partial fulfilment of the requirements for the degree of

Master of Science (MSc)

Wien, 2021 / Vienna 2021

Studienkennzahl lt. Studienblatt / degree programme code as it appears on the student record sheet:	A 066 863
Studienrichtung lt. Studienblatt / degree programme as it appears on the student record sheet:	Masterstudium Biologische Chemie UG2002
Betreut von / Supervisor:	Univ.-Prof. Dr. Christopher Gerner
Mitbetreut von / Co-Supervisor:	Dott. ric. Giorgia Del Favero, Privatdoz.

Abstract

Ovarian cancer is one of the most lethal malignancies among women. It is a disease with a generally unfavorable outcome due to late diagnosis, and late stage ovarian cancer has typically already started to metastasize. For advanced stage ovarian cancer, the usual care is surgery and platinum-based chemotherapy, whereby most patients experience a relapse of cancer, and a recurring ovarian cancer is not curable, which can be attributed to a developed chemoresistance. Based on current knowledge, two well-known factors contribute significantly to the development of chemoresistance in ovarian cancer, namely hypoxia and shear stress. Hypoxia regulates many signaling pathways and thus cancer growth and influences post-translational modifications of various proteins. Shear Stress impacts morphology, expression of biomarkers, and aggressiveness of tumor cells, providing an ideal tumor microenvironment. Both hypoxia and shear stress are though to affect mitochondrial morphology and protein composition of the electron transport chain

Within this thesis, two human ovarian cancer cell lines (SKOV-3 and OVCAR-3) were subjected to the oxygen level (hypoxia) or the biophysical stimulation (shear stress) of an ovarian cancer environment to mimic the *in vivo* situation more accurately. Cells were microscopically monitored and imaged prior and after the respective treatments, to subsequently evaluate the morphological alterations with respect to area, perimeter, major and minor axes, circularity, and roundness of the cells. Furthermore, proteomic alterations were determined using mass spectrometric analysis (cell lysis, proteolytic digestion, and LC-MS/MS), and finally, regulated proteins and thus the affected signaling pathways were identified by bioinformatic analysis. Depending on the proteomic analysis (untargeted proteomic or phosphoproteome analysis), cells were treated for 24 h (long-term) or 3 h (short-term), respectively.

For both cell lines, morphological as well as proteomic alterations could be determined after 24 h treatment in the respective experimental condition, with identified proteins consistent with and exceeding those reported in literature. Based on the 3 h incubations, the different treatment groups (hypoxic, shear stress, and normoxic static control) could only be vaguely separated from each other via PCA, and almost no regulated proteins could be identified in the basic proteomic profiles of both cell lines. An exhaustive molecular interpretation and discussion of the proteomics data is beyond the scope of this master's thesis, as the aim was to create a suitable experimental design and to gain first insights into the impacts of artificial hypoxia and fluid shear stress using the respective methods on ovarian cancer cell lines. In conclusion, we identified significant morphological and proteomic (untargeted as well as phospho-proteomic) alterations for both cells lines after both treatments compared to the control cells, suggesting the methods are suitable for mimicking the ovarian cancer microenvironment more adequately.

Zusammenfassung

Eierstockkrebs gehört zu den tödlichsten malignen Erkrankungen bei Frauen, mit einem allgemein ungünstigen Krankheitsverlauf, aufgrund der üblicherweise späten Diagnose. Spät diagnostizierter Eierstockkrebs bedeutet in der Regel auch ein fortgeschrittenes Stadium und hat meist bereits Metastasen gebildet. Die herkömmliche Behandlung für progressiven Eierstockkrebs umfasst einen chirurgischen Eingriff und eine platinhaltige Chemotherapie, wobei der Großteil der Patientinnen einen Rezidiv erleidet und ein wiederkehrender Eierstockkrebs aufgrund einer entwickelten Chemoresistenz nicht mehr heilbar ist. Für die Entwicklung dieser Chemoresistenz bei Eierstockkrebs gelten zwei Faktoren als besonders entscheidend, nämlich Hypoxie und fluide Scherbelastung. Hypoxie reguliert viele Signalwege und somit auch das Krebswachstum, und beeinflusst posttranslationale Modifikationen verschiedener Proteine. Scherbeanspruchung beeinflusst die Morphologie, die Expression von Biomarkern und die Aggressivität von Tumorzellen, und bietet so eine ideale Mikroumgebung für Tumore. Sowohl Hypoxie wie auch fluide Scherbelastung wird eine Auswirkung auf die mitochondriale Morphologie und die Proteinzusammensetzung der Elektronentransportkette zugesprochen.

Im Rahmen dieser Arbeit wurden zwei menschliche Eierstockkrebs-Zelllinien (SKOV-3 und OVCAR-3) dem Sauerstoffgehalt (Hypoxie) oder der biophysikalischen Stimulierung (Scherbeanspruchung) des Milieus eines Eierstockkrebses ausgesetzt, um die tatsächliche Umgebung, wie sie *in vivo* ist akkurater zu imitieren. Die Zellen wurden vor und nach den jeweiligen Behandlungen mikroskopisch überprüft und abgebildet, um anschließend die morphologischen Veränderungen in Hinblick auf Fläche, Umfang Haupt- und Nebenachsen, Zirkularität und Rundheit der Zellen zu evaluieren. Des Weiteren wurden proteomische Veränderungen mittels Massenspektrometrie (Zellaufschluss, proteolytische Spaltung und LC-MS/MS) bestimmt, und schließlich wurden regulierte Proteine und folglich die betroffenen Signalwege durch bioinformatische Auswertung ermittelt. Je nach Art der Proteom-Analyse (ungezielte Proteom-Analyse oder Phospho-Proteom-Analyse) wurden die Zellen für 24 Stunden (Langzeit) beziehungsweise für 3 Stunden (Kurzzeit) den beiden Bedingungen ausgesetzt.

Es konnten für beide Zelllinien unter jeder Versuchsbedingung nach 24-stündiger Behandlung sowohl morphologische als auch proteomische Veränderungen ermittelt werden, mit Proteinidentifikationen, die mit denen in der Literatur beschriebenen übereinstimmen und darüber hinausgehen. Ausgehend von den 3-stündigen Inkubationen konnten die verschiedenen Behandlungsgruppen (hypoxisch, scherbeansprucht, und normoxische statische Kontrolle) mittels PCA nur vage voneinander getrennt werden, und in den grundlegenden proteomischen Profilen beider Zelllinien konnten fast keine regulierten Proteine identifiziert werden. Eine ausführliche molekulare Interpretation und Diskussion der Proteomik Daten würde den Rahmen dieser Masterarbeit überschreiten, da das Ziel die Erstellung eines geeigneten Experimentaufbaus und erste Erkenntnisse über die Auswirkungen von künstlicher Hypoxie und fluider Scherbelastung auf Ovarialkarzinom-Zelllinien mit den jeweiligen Methoden war. Zusammenfassend konnten wir für beide Zelllinien nach beiden Behandlungen im Vergleich zu den jeweiligen Kontrollzellen signifikante morphologische und proteomische (ungezielte sowie Phospho) Veränderungen feststellen. Dies deutet darauf hin, dass die eingesetzten Methoden zur Nachahmung der Mikroumgebung eines Eierstockkrebses geeignet sind.

Acknowledgments

First, I would like to thank Univ.-Prof. Dr. Christopher Gerner for the opportunity to do my master's thesis at the Department of Analytical Chemistry in his research group. Next, I would like to thank Dott. Ric. Giorgia Del Favero (Department of Food Chemistry and Toxicology) for the co-supervision of my thesis, the availability of her equipment and her great support. I am incredibly grateful to both for the possibility to do research on this exciting and important topic and project, as it has a very important meaning for me personally.

Furthermore, I thank Benjamin Neuditschko for his supervision and support in cell culture and proteomics during my entire time in lab. He taught me several important techniques and procedures and was always patient with me, friendly and helpful.

Thanks also to Eva Attakpah and Dr. Endre Kiss, former technician and technician at the Department of Food Chemistry and Toxicology, who always supported me in all aspects of the technical processes and patiently instructed me in the use of various devices.

Special thanks to Dr. Esther Heid for her ideas and support with the calculations for the shear stress experiments. The conversations with her were extremely inspiring and motivating.

In addition, I would like to thank the entire Gerner working group for their help and support, but especially Gaurav Mitra and Gerhard Hagn for their guidance and assistance with protein digestions.

Once again, I would like to thank Dott. Ric. Giorgia Del Favero, as she introduced me to the world of cell culture and imaging when I was a bachelor student and I basically owe my techniques and knowledge to her. I thank her from the bottom of my heart for her warm nature and enthusiasm, which has always motivated and cheered me. Of course, I also thank her for all the stimulating conversations, her vast knowledge she shared with me and her full support I received throughout.

Last but not least I want to thank my parents for their unconditional support during the entire time and their understanding whenever I had to take a break. Mom and Dad always motivated me and helped me wherever they could and made me who I am today. Thanks to you I am where I am today!

Table of contents

List of abbreviations

1D	One-dimensional
2-CAM	2-Chloroacetamide
2D	Two-dimensional
3D	Three-dimensional
AA	Amino acid
ABC	ATP-binding cassette
ACN	Acetonitrile
ADP	Adenosine diphosphate
APAF1	Apoptotic protease activating factor 1
APCI	Atmospheric pressure chemical ionization
APPI	Atmospheric pressure photon ionization
ATP	Adenosine triphosphate
BCA	Bicinchoninic acid
BSA	Bovine serum albumin
BSO	Bilateral salpingo-oophorectomy
BU	Bottom-up
CAV1	Caveolin 1
CI	Chemical Ionization
CID	Collision-induced dissociation
CSCs	Cancer stem cells
CYT	Cytoplasmic fraction
DMSO	Dimethylsulfoxide
DNA	Deoxyribonucleic acid
DTT	Dithiothreitol
EDTA	Ethylenediaminetetraacetic acid
EGFR	Epidermal growth factor receptor
EGTA	Ethylene glycol-bis (2-aminoethyl ether)-N, N, N’, N’-tetraacetic acid
EI	Electron Ionization
ELISA	Enzyme-linked immunosorbent assay
EMT	Epithelial mesenchymal transition
EP	EasyPhos
ER	Endoplasmic reticulum
ERK	Extracellular signal-regulated kinases
ESI	Electrospray ionization
FA	Formic acid

FAB	Fast atom bombardment
FAK	Focal adhesion kinase
FCS	Fetal calf/bovine serum
FDR	False discovery rate
FT-ICR	Fourier-transform ion cyclotron resonance
GTP	Guanosine triphosphate
HCD	Higher energy collisional dissociation
HEPES	4-(2-Hydroxyethyl)-1-piperazineethanesulfonic acid
HGSOC	High grade serous ovarian cancer
HIF-1α	Hypoxia-inducible factor 1α
HPLC	High performance liquid chromatography
IAA	Iodoacetamide
IEF	Isoelectric focusing
IGF1R	Insulin-like growth factor 1 receptor
IMAC	Immobilized metal ion affinity chromatography
IMS	Ion mobility spectrometry
IT	Ion trap
iTRAQ	Isobaric tags for relative and absolute quantification
Jak1	Janus kinase 1
LB	Lysis buffer
LC	Liquid chromatography
LC-MS	Liquid chromatography mass spectrometry
LFQ	Label-free quantification
LTQ	Linear trap quadrupole
m/z	mass-to-charge ratio
MALDI	Matrix assisted laser desorption ionization
MAPK	Mitogen-activated protein kinase
MDR	Multidrug resistance
mRNA	Messenger ribonucleic acid
MS	Mass spectrometry
MS/MS	Tandem mass spectrometry
NE	Nuclear extract
NFκB	Nuclear factor kappa-light-chain-enhancer of activated B cells
NMR	Nuclear magnetic resonance
NP-40	Nonidet P-40 (4-nonylphenyl-polyethylene glycol)
OC	Ovarian cancer

p-sites	Phosphorylation sites
PAGE	Polyacrylamide gel electrophoresis
PARP	Poly(ADP-ribose)-polymerase
PASEF	Parallel accumulation serial fragmentation
PBS	Phosphate buffered saline
PCA	Principal component analysis
Pgp	P-glycoprotein
PI3K	Phosphoinositide 3-kinase
PKC	Protein kinase C
PLOD	Procollagen-lysine 2-oxoglutarate 5-dioxygenases
PMSF	Phenylmethylsulfonyl fluoride
PPC	Protease and Phosphatase Inhibitor Cocktail
pS	Phosphoserine
pT	Phosphothreonine
PTM	Post-translational modification
P/S	Penicillin-Streptomycin
pY	Phosphotyrosine
Q	Quadrupole
QQQ	Triple quadrupole
RNA	Ribonucleic acid
RT	Room temperature
SDC	Sodium deoxycholate
SDS	Sodium dodecyl sulfate
SILAC	Stable isotope labeling by/with amino acids in cell culture
TCEP	Tris(2-carboxyethyl)phosphine
TD	Top-down
TE	Tris/HCl EDTA
TEAB	Triethylammonium bicarbonate
TFA	Trifluoroacetic acid
TIMS	Trapped ion mobility spectrometry
TME	Tumor microenvironment
TMT	Tandem mass tags
TOF	Time of flight
Tris/HCl	Tris(hydroxymethyl)aminomethane-hydrochloride
VEGF	Vascular endothelial growth factor
WB	Western blot

1. Introduction

1.1. Ovarian cancer

Ovarian Cancer (OC) is actually only ranked 3rd among gynecologic cancers in women worldwide, but it is the most lethal one [1]. The fatality of OC is partly attributed to late diagnosis, meaning OC is usually diagnosed at an advanced stage, also defined as stage III or IV. This is due to very modest symptoms, even though the tumor has already started to metastasize. Therefore, OC is also called the silent killer. [2-4] To put it into numbers, OC has a 5-year survival rate of about 30% for stage III and 15% for stage IV disease. When diagnosed early, stage I or II, OC has a more favorable outcome. [1] Mortality of OC depends not only on the stage at which it is diagnosed, but also on a patient's age, and the frequency of occurrence depends as well on the patient's age. The older the age, the higher the incidence and mortality of the disease. Furthermore, from the age of 75, the probability of both incidence and mortality increases to over 50%. [5] Apart from advanced age, the major risk factors are family history and genetic predisposition, numerous ovulations, endometriosis, dietary factors, and modestly ethnicity [2]. In contrast, the following factors reduce the risk of developing OC, namely pregnancy, breast-feeding, early menopause, multiparity, hysterectomy, late menarche, low-fat diet, use of the oral contraceptive pill (hence ovulation suppression), and tubal ligation [5, 6].

Further, the nature of OC, which is reflected in the histopathology, contributes to the fatality of the disease. It is necessary to distinguish between epithelial, germ cell, and sex-cord-stromal types, with epithelial OC being the most common type, which in turn is divided into four histological subtypes (summarized in Table 1). In addition, epithelial tumors are divided into type I and type II to indicate the level of lethality. Type I tumors are those with a better prognosis, are not that lethal, and are typically diagnosed at an early stage, while type II tumors are the ones with a usually fatal outcome, late diagnosis and linkage to genetic mutations, e.g. of the BRCA and p53 genes. [2] Mutations in the BRCA genes are attributed as the strongest association with OC risk, with BRCA1 mutations associated at 50% and BRCA2 mutations at just 20%. Overall, genetics is thought to be implicated in 10-15% of all OC incidences. [6]

Table 1 Subtypes of epithelial ovarian cancer.

Serous tumors	
High-grade serous carcinomas (HGSC) • 70-80% of all subtypes • More fatal prognosis • 10-year mortality rate of 70%	Low-grade serous carcinomas (LGSC) • < 5% of all subtypes • Diagnosed at younger age • Better prognosis than HGSC
Endometrioid carcinomas • 10% of epithelial OCs • Originate from endometriosis • Good prognosis	
Clear cell carcinomas • 10% of epithelial OCs • Good prognosis when diagnosed in early stage → often • Poor prognosis when diagnosed late	
Mucinous carcinoma • 3% of epithelial OCs → least common type • Associated with metastasis from gastrointestinal tract	

There is no commonly agreed pathogenesis of OC, and this can be attributed to the heterogeneity of OC, meaning the already mentioned different histological types, which also differ in their behavior and characteristics. Different theories are available for the origin of OC, such as the incessant ovulation theory, the fallopian tube theory, and the two-pathways theory. According to the incessant ovulation theory, all OCs have their origin in the epithelium of the ovarian cell surface which would explain the increasing risk of OC in relation to the number of ovulatory cycles. However, there is no feasible explanation for the different histologic types (e.g., serous, endometrioid, mucinous) and the prognostic differences. Moreover, the increased risk for women with polycystic ovary syndrome is not consistent with this theory. Based on the fallopian tube theory, OC is thought to originate in the fallopian tube and then migrate to the adjacent ovary. Consideration of the histologic, clinical, and genetic evidence of OC (type I and II) led to the two-pathways theory. Here, type I OC, in which KRAS and BRAF mutations that can activate the mitogen-activated protein kinases (MAPK, originally known as extracellular signal-regulated kinases (ERK)) pathway are the most prevalent, arise from the epithelium of the ovarian surface. In contrast, type II OC is thought to arise from outside the ovary, such as from the fallopian tube. As mentioned before, type II OCs are usually associated with p53 and BRCA gene mutations and therefore proliferate more aggressively. Figure 1 provides an overview of the two-pathways theory. [4, 6-9]

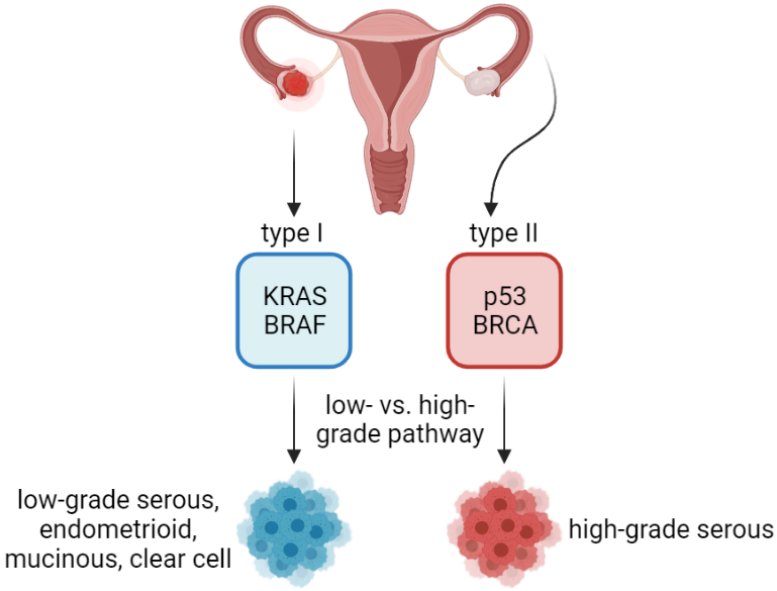

Figure 1 The two-pathway theory of epithelial ovarian cancer development. Derived and modified from Budiana *et al.* 2018 [6] and created with BioRender.com.

Furthermore, different types of tumors spreading behavior in OC have been described, miliary and non-miliary. The miliary type is defined by widespread and millet-sized implants in the peritoneal cavity and is further associated with poor prognosis. In contrast, the non-miliary type is characterized by larger but less frequent implants and is related to a more favorable prognosis. [10-12] This distinction in spreading behavior is consistent with the idea of the two-pathways theory. The more aggressive spreading type (miliary) seems to occur when OC originates from outside the ovary according to the fallopian tube theory (type II OC). In turn, this implies the non-miliary type can be assigned to type I OC, i.e., those tumors presumed to originate in the epithelium of the ovarian surface. [10, 12] Non-miliary spread is

thought to be genuine metastasis via blood or lymphatic system. For the miliary type, it would be possible that cells have colonized in the peritoneum as they migrated through it toward the ovary. [12]

Depending on the histological type of tumor, treatment and/or prognosis can differ. Moreover, time of diagnosis, i.e., at which stage OC is diagnosed, plays a major role, but diagnosis at an early stage is rather uncommon in OC due to vague and non-specific symptoms. The most common symptoms are shown in Table 2. [2, 5]

Table 2 Best known presenting symptoms of ovarian cancer, listed in descending order.

<table>
<tr><td colspan="2">Abdominal pain</td></tr>
<tr><td colspan="2">Swelling (increased abdominal size)</td></tr>
<tr><td>Gastrointestinal symptoms
• Nausea
• Vomiting
• Constipation
• Diarrhea</td><td>Gynecological symptoms
• Unusual bleeding
• Pain in genital region</td></tr>
<tr><td colspan="2">Pelvic pain</td></tr>
<tr><td colspan="2">Bloating</td></tr>
<tr><td colspan="2">Difficulty in eating and/or early satiety</td></tr>
<tr><td colspan="2">Back pain</td></tr>
<tr><td colspan="2">Fatigue</td></tr>
<tr><td colspan="2">Urinary symptoms</td></tr>
</table>

For years, the usual treatment for OC is surgical resection followed by chemotherapy consisting of a combination of platinum (carboplatin) and non-platinum (paclitaxel) agents. Debulking surgery is typically accompanied by hysterectomy and bilateral salpingo-oophorectomy (BSO). If necessary, the pelvic and para-aortic lymph nodes, and the omentum are removed as well. In some cases, a supplementary appendectomy is performed, as the appendix is often site of OC metastasis. [2, 5] Apart from surgical removal due to diagnosed OC, there are also preventive surgeries, such as BSO, tubal ligation, or removal of fallopian tubes. These are performed in women with a genetic predisposition (e.g., BRCA1 mutation) as a risk-reducing step. [2, 4, 8, 9] In addition to surgical prevention, there are potential pharmaceutical preventions, but these are controversial just as neoadjuvant therapies are. Promising new adjuvant agents are available, such as poly(adenosine diphosphate (ADP)-ribose)-polymerase (PARP) inhibitors, which prevent cancer cell regeneration after chemotherapy. [2, 13, 14]

Unfortunately, there are far too many relapses of OC, and it is a challenge to treat a recurring OC. The usual objective of repeated surgical therapy is to relieve the symptoms, but life-prolonging surgeries (cytoreduction) exist as well, although there is simply no known cure for relapsed OC. [15]

1.1.1. Drug resistance

The lack of a known cure for relapsed OC can largely be attributed to developed chemoresistance. [16] Development of chemoresistance may occur during treatments with chemotherapeutic agents, when normal cells are supposed to recover, and exactly then, cancer cells and cells within the

microenvironment can recover and thus mutate into chemoresistant and much more aggressive cancer cells. [13] Characteristics of OC, such as its heterogeneity, contribute to its resistant nature: [17] Indeed, several mutations have already resulted in PARP inhibitor resistance. [14] It is reported, that the overexpression of epidermal growth factor receptor (EGFR) is associated with the aggressiveness and drug resistance of OC. [18] Moreover, the development of multidrug resistance (MDR) is directly linked to overexpression of the transmembrane protein P-glycoprotein (Pgp), an adenosine triphosphate (ATP)-dependent pump, which pumps diverse drugs, including chemotherapeutics, outside cells. [19] ATP-binding cassette (ABC) transporters in general, which include the ATP-dependent pump, contribute to the development of anticancer drug resistance by effusing drugs out of cells. [20] There is strong evidence that cysteine plays a crucial role in resistance to carboplatin in OC cells. [21]

In general, according to current knowledge, the development of chemoresistance in OC is promoted by two important factors, namely hypoxia and shear stress. [22-24]

1.1.2. Hypoxia

Hypoxia is typical for aggressive carcinomas and promotes angiogenesis, metastasis, and invasiveness of tumors [17, 24, 25] by stimulating vascular endothelial growth factor (VEGF) release. [26] The most prominent transcription factor in oxygen regulation of cells is hypoxia-inducible factor 1α (HIF-1α), which is highly expressed under hypoxia and impacts cell proliferation as well as invasion and metastasis by activating more than 100 downstream genes, including those for angiogenesis. [25-28]

For OC cells, it can be stated equally that hypoxia causes a more invasive nature, makes cells more capable of migration, and the cells show a change in epithelial mesenchymal transition (EMT). [24] It is widely known that the hypoxic microenvironment of cancer cells contributes to chemoresistance in OC, but the exact mechanism has not been fully elucidated. [22]

Diverse studies identified a variety of regulations in OC cells induced by hypoxia, such as down-regulation of the apoptotic protease activating factor 1 (APAF1) through overexpressed miR-27a [22], the epithelial marker E-cadherin [29], and caveolin 1 (CAV1, a potential tumor suppressor) [30], or activation of insulin-like growth factor 1 receptor (IGF1R) [17], or up-regulation of the mesenchymal marker Vimentin, the transcription factor SNAIL1 [29], the Janus kinase 1 (Jak1, a tyrosine kinase linked to cisplatin resistance) [30, 31], and procollagen-lysine 2-oxoglutarate 5-dioxygenases (PLOD) 1 and 2 [32]. APAF1 protein was shown to be a key regulator of apoptosis, so down-regulation helps cancer cells to escape apoptosis, and its suppression contributes to cell proliferation and anticancer drug resistance in OC. [33-35] Other widely known hypoxia-induced regulations are the phosphoinositide 3-kinase (PI3K), MAPK/ERK, and nuclear factor kappa-light-chain-enhancer of activated B cells (NFκB) pathways. [36]

A couple of previous reports have revealed that hypoxia-induced resistance to chemotherapy is reversible quite fast once the cells are reoxygenated to normoxic conditions. [37-39] It was demonstrated by McEvoy *et al.* 2015 that for chemoresistance the hypoxic condition must be present at time of treatment, and prior hypoxia alone does not account much. [30]

1.1.3. Shear stress

Apart from chemical signals, such as reduced oxygen levels, physical forces act on cells in a living organism and thus also on cancer cells. It is necessary to distinguish between solid and fluid forces, with fluid stress consisting of factors such as microvascular fluid pressure, interstitial fluid pressure, and fluid shear stress caused by the blood flow and/or interstitial flow. [40] Fluid shear stress is also present in the peritoneum, and ascites, also known as ascitic fluid, represent the accumulation of protein-rich material in the peritoneal cavity and are frequent features of OC, providing a tumor microenvironment (TME) with mitogenic growth factors, creating ideal conditions for tumor progression. [21, 41] The physiological conditions in the peritoneal fluid, pressure, strain, and shear stress, which in turn are also characteristics of ascitic fluid, can affect the morphology, the expression of biomarkers, and the aggressiveness of tumor cells. [41, 42] Fluid shear stress not only provides an ideal TME for tumor growth, but also contributes to spreading of OC and may favor the accumulation of cancer stem cells (CSCs). [42] It has been described that physical factors have a greater impact on the distribution pattern of cancer cells within ascites than the biological ones. [43]

Further, it is believed that the physical stress caused by ascitic fluid has an impact on the drug resistance in (metastatic) OC. Nath *et al.* 2020 demonstrated increased resistance toward carboplatin in OC cells when cultivated under flow-induced shear stress. In addition, they observed an upregulation of EGFR and the MAPK/ERK pathway which are widely known to be associated with treatment resistance. [23] The results of Ip *et al.* 2016 showed that OC cells grown under fluid shear stress developed a chemoresistance to cisplatin and paclitaxel. Furthermore, these findings suggest a mechanism for the development of MDR which is ABCG2 and/or Pgp dependent. [42] The most common type of metastasis in OC is transcoelomic metastasis (Fig. 2), which is mainly favored by ascitic fluid and related biomechanical stimuli, and the preferred sites for OC metastasis are the peritoneum, the greater omentum, the right subphrenic region, the lung, and the liver. [44-46]

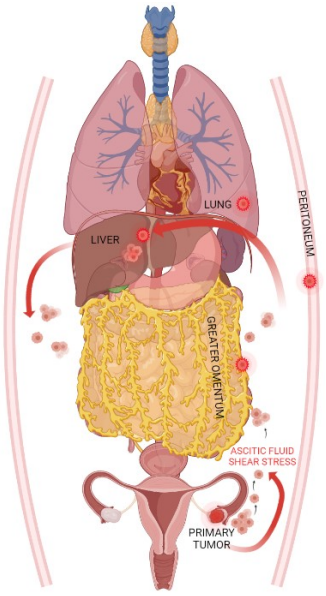

Figure 2 Transcoelomic metastasis of ovarian cancer initiates with detachment of cells from the primary tumor due to ascitic fluid shear stress Ovarian cancer cells in ascites escape the immune system and pass through the ascitic stream as spheroids to sites of metastasis (here indicated: omentum, peritoneum, liver, and lung). Derived and modified from Novak *et al.* 2018 [44] and created with BioRender.com.

1.2. Proteomics

Proteomics is the counterpart to genomics at protein level and deals with the totality of proteins, the proteome, and how they interact with each other and in the organism. Marc Wilkins defined the term “proteome” within a symposium in 1994. [47] Proteins are composed of a specific sequence of amino acids (AA) determined by the nucleotide sequence of the Deoxyribonucleic acid (DNA), which is first transcribed into ribonucleic acid (RNA), further processed into messenger RNA (mRNA), and then translated into proteins. The information in the genome, including mutations, the start site of translation with the open reading frame, and post-translational modifications (PTMs) determine the AA sequence as well as the structure and chemistry of a protein. [48] The number of proteins within an organism seems to be constant, like the genome is, but in fact proteins are continuously produced and disassembled, and this very dynamic nature of the proteome makes it necessary to always refer to the tissue or cell type, or even to consider the age of the organism, as the proteome changes with advancing maturity. [49, 50] Proteins govern the structure and activity of cells, affect signaling pathways, coordinate chemical reactions and thus metabolism. Their proper function is largely ensured by their structure, and a deficiency can be responsible for disorders such as Huntington’s disease which causes dementia. [48] With proteomics, a much more accurate description or statement regarding a functioning cell can be made than with genomics alone, as protein interactions not only provide insights into functions of individual proteins, but also into their roles in signaling pathways, networks, and complexes. [51] A major benefit is the utilization of proteins as healing or adjuvant agents, such as antibodies against viral or bacterial infections. [48]

Although the term “proteomics” was not defined before the 1990s, the very first proteomic analysis was performed in 1975 with the mapping of proteins using two-dimensional (2D) gel electrophoresis, implemented by O’Farrell [52], Klose [53], and Scheele [54], but these proteins could not be identified then. [50, 55] Years earlier, in the late 1940s, the Edman degradation, in which AA after AA is removed via chemical reaction, was used for identification of the first protein sequences. [50, 51, 56] Due to the lengthy and laborious work required to identify proteins as well as the facts that no N-terminal modifications, such as acetylation, may be present and peptides may consist of a maximum of 30 AAs, this method is severely limited in its efficiency. [48, 51, 57] Shortly before the term “proteomics” was born, the mass spectrometry (MS) was made suitable for protein identification analysis by introducing soft ionization methods, with matrix assisted laser desorption ionization (MALDI) and electrospray ionization (ESI) being quite prominent. Due to certain advantages compared to Edman sequencing, namely improved sensitivity, capability to analyze protein mixtures, and suitability for high-throughput analysis, MS is the tool of choice for the last decades. [50, 51, 58] The improved sensitivity and accuracy of MS enable reliable analyses down to attomole range. [59]

There is a need to distinguish between “identifying” and “comparative” proteomics. In the former, the aim is to identify the proteins that constitute a sample (ideally a proteome), whereas in comparative proteomics, the intention is to examine the proteins within a sample in relation to another one. [49] In general, proteomics can be divided into different subfields, which are shown in Table 3. [48-51, 57]

Table 3 Subfields of proteomics and their implementations.

Subfield	Determination/Identification of
Protein identification	AA sequence
Protein quantification	Protein amount at any given time
Protein localization	Expression site (cellular localization/cell type)
Protein modifications	Post-translational modifications • Glycosylation • Phosphorylation • Acetylation • Methylation • Ubiquitination → degradation
Functional proteomics	Biological functions • Distinct proteins • Protein classes • Protein complexes/networks
Structural proteomics	Protein structure • 3D structure • Protein complexes/networks • Organelle composition
Interaction proteomics	Protein-protein interactions • Which proteins • When • Where

Since protein functions are affected by their structure, which in turn is determined by their AA sequence, it is logical that the function of a protein is related to its AA sequence, and hence, apart from x-ray crystallography and nuclear magnetic resonance (NMR) spectroscopy, there is prediction of structures, which contributes greatly to the field of three-dimensional (3D) protein structure analysis. For this purpose, there are meanwhile several protein databases, such as Swiss-Prot, established in 1986. [51]

Beyond the subfields of proteomics, the different proteomic techniques/methods, low-throughput vs. high-throughput methods, need to be distinguished (compare Table 4). The best known methods for detecting distinct proteins using probes (antibodies, immunoassays) are Western blot (WB) [60] and enzyme-linked immunosorbent assay (ELISA), but these techniques are rather limited in their efficiency. [48, 61] Other well-known methods are gel electrophoreses, which are primarily used for separation of protein mixtures, but can also be used for identification, although it is not very specific. One-dimensional (1D) gel electrophoresis separates proteins according to their mass (10 to 300 kDa), and thus it is quite easy to “misidentify” them, as identification is done by simply comparing masses and several proteins (may) have the same mass. Whereas the 2D gel electrophoresis separates protein mixtures first by their isoelectric point (isoelectric focusing, IEF) and then in the second dimension by their mass, making misidentification less likely, and even whole cell lysates can be separated using this technique. [50, 51, 60] Next level for separating protein mixtures is (multidimensional) liquid chromatography (LC), in which proteins as well as peptides can be separated by size, charge, hydrophobicity and/or affinity for certain ligands, but also purified. Additional advantages are increased sensitivity and the ease of

automatization, and the option to perform a downstream MS analysis. [51, 62] There are other chromatographic methods available, however, they are not as common in the field of proteomics. Protein chips (microarrays), including antibody and antigen chips, are suitable for multiple applications such as quantitative or functional proteomics. Antibody chips use a set of antibodies to detect a specific protein within a sample, both qualitatively and quantitatively. Antigen chips, in contrast, are used for the detection and quantification of antibodies with the aid of antigens. Further types of protein microarrays are universal protein chips (functional arrays, such as lectin arrays used for detection and characterization of glycoproteins), protein capture chips (using other molecules to capture proteins by interaction), and solution arrays. [51, 63] With MS, proteins are identified not only by mass, but by their mass-to-charge ratio (m/z) or by their velocity (flight time), i.e., peptides and AA sequences are detected rather than proteins, and the identification of proteins is based on database search. Each MS analysis consists of a preliminary sample preparation, ionization, and subsequent mass analysis. For years, MALDI and ESI are both ionization techniques of choice in proteomics. There are also a variety of mass analyzers available, with the most important to know being the quadrupole (Q, m/z analyzer), time of flight (TOF, velocity), and ion trap (IT, m/z). [50, 57, 64]

Table 4 Proteomic techniques and their allocation: low-throughput vs. high-throughput methods.

Low-throughput methods	**High-throughput methods**
Immunoassays (using antibodies) • WB • ELISA • Chemiluminescence	Microarrays • Antibody chips • Antigen chips • Universal chips → functional • Protein capture chips • Solution arrays
Gel electrophoresis • 1D • 2D	Mass spectrometry • MALDI • ESI
Chromatography • LC	

Moreover, a distinction between bottom-up (BU) and top-down (TD) proteomics is necessary, with the main difference between these two methods in MS being the sample preparation prior to ionization, namely in BU the proteins to be analyzed are digested, and in TD intact proteins (< 70 kDa) are analyzed. For intact proteins the ionization is more complex than for peptides, and a higher resolution is required. [65] The method of choice in proteomics is currently BU-MS (also called shotgun-proteomics respectively MS), in which proteins are digested enzymatically as part of sample preparation, and subsequently the obtained peptides (0.8 to 3 kDa) are ionized, their masses are analyzed and thus the proteins are identified. [48]

1.2.1. Shotgun-Proteomics

In shotgun-proteomics (or BU-proteomics), the goal is the identification of proteins within a complex sample (e.g., complete cell lysate) by analyzing their constituent peptides using tandem mass spectrometry (MS/MS). The proteins are commonly digested into peptides with the protease trypsin prior to ionization, then ionized with a method of choice, and subsequently separated according to their m/z. The separated peptides are detected, then the most abundant ones are fragmented, and in turn the fragments are detected to determine the AA sequences of the peptides. Thus, in shotgun proteomics peptide fragments are analyzed, while in TD proteomics fragments of proteins are analyzed (compare Fig. 3). To determine the analyzed proteins, both methods require as last step the database search. [48]

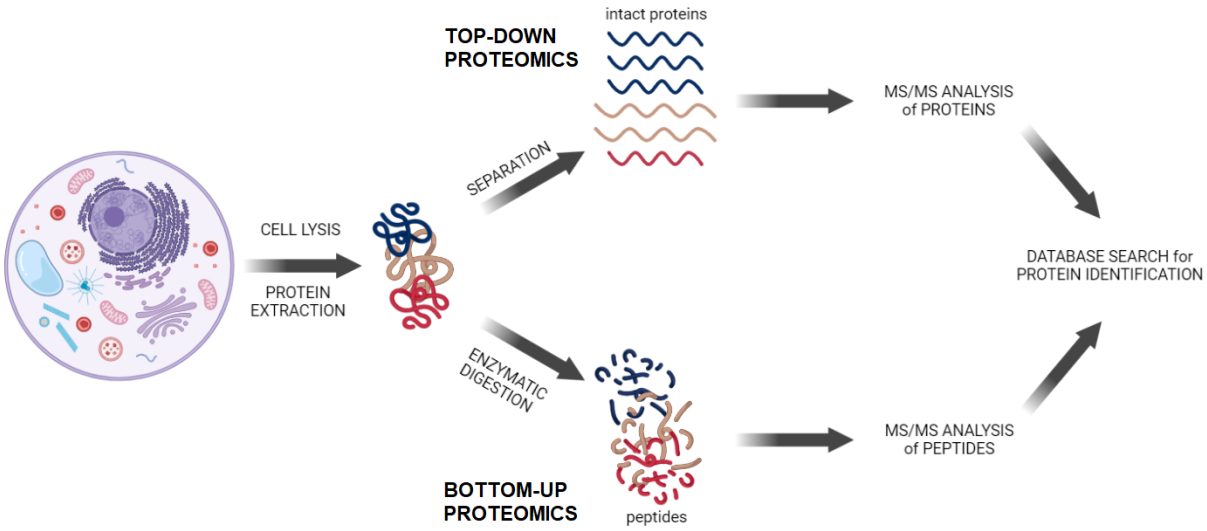

Figure 3 General depiction of the methodologies in proteomics with the comparison of bottom-up vs. top-down proteomics, created with BioRender.com

To reduce complexity of a sample, additional separation steps are frequently carried out as part of sample preparation. The preferred method for protein separation in the early days was 2D polyacrylamide gel electrophoresis (PAGE), where the proteins were cut out of the gel after separation to be analyzed and identified by MS. [50] Another commonly used method to reduce sample complexity before ionization, is the already mentioned LC. [48, 57, 64] Some ionization techniques, such as ESI, need purified peptides for proper operation, therefore LC and ESI were combined, and the purified ionized samples were automatically loaded to the MS. [50, 57] Commonly a combination of high performance liquid chromatography (HPLC) with MS is used. [66, 67]

The analysis or detection of the masses of separated peptides is also referred as peptide mass fingerprinting and results in mass spectra of peptides, also referred as MS1 spectra. On the other hand, the detection of the masses of peptide fragments is referred as AA sequencing and results in MS2 spectra (MS/MS spectra, fragment spectra). [50] With these spectra, the already mentioned database searches are performed, resulting in protein identification. However, it must be considered that a significant number of spectra (about 75% [68]) cannot be properly identified due to low signal-to-noise ratios, incompleteness of available databases, or unexpected PTMs, and therefore do not yield any results, compromising the sensitivity of shotgun proteomics. [48]

1.2.2. Phospho-Proteomics

Phospho-proteomics belongs to the proteomics subfield of protein modifications, in which PTMs, such as glycosylation or phosphorylation (see Table 3), are determined and characterized. Increasing focus on protein phosphorylations and thus phospho-proteomics is emerging to gain a better understanding of diverse signaling pathways and hence cellular functions [69], as phosphorylations are the most common PTMs. [70] Furthermore, phosphorylations are the most investigated PTM as they regulate a range of cellular functions (cell growth, differentiation, apoptosis, and cell signaling), and variations in the mechanism and thus phosphorylation patterns can cause severe consequences and may contribute to the development of disease. [71]

BU-MS is favored for the analysis of protein modifications due to its sensitivity and ability to provide both quantitative and site-specific information. Dedicated MS techniques have been developed to enable the scanning of specific PTMs, though in the case of phospho-proteomics in particular, challenges interfere with flawless analysis. [64] Using MS, it was revealed that the majority of proteins are phosphorylated, and indeed at multiple sites. [72] The exact numbers of phosphorylated proteins and phosphorylation sites (p-sites) for humans are still not determined, with approximately 70-95% of total phosphoproteins and 40-60% of p-sites being known. [70] Several databases are available providing information on PTMS, such as UniProt [73], PhosphoSite [74], and PHOSIDA [75]. [76]

In the early 2000s, it was believed that there are about 200 different types of PTMS. [50] Minguez *et al.* 2012 mentioned over 400 different PTMs were listed in the UniProt database and described the connectivity of the different types, showing that in humans alone, more than 50,000 residues in about 6,000 proteins are modified, with phosphorylation being the most frequent PTM, followed by N-linked glycosylation and acetylation, respectively. [76] Phosphorylation is the addition of a phosphate group (PO_4) by kinases and is a reversible mechanism, known as dephosphorylation mediated by phosphatases, see Fig. 4. ATP serves as phosphate group donor, and after phosphorylation, the protein may change its conformation or is able to form bonds and thus assemble or disassemble protein complexes. [77]

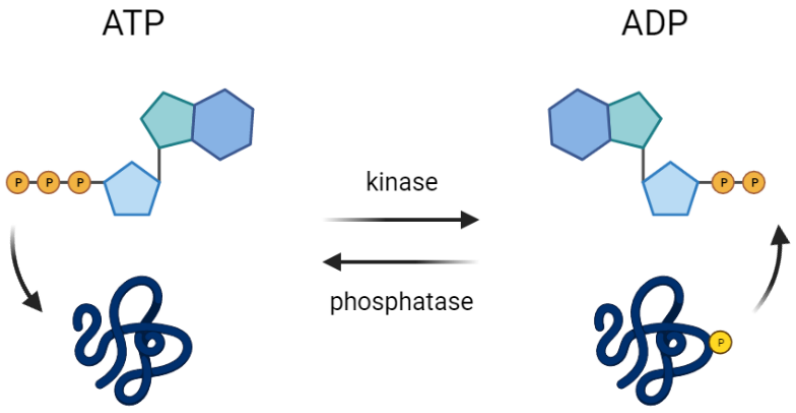

Figure 4 Scheme of phosphorylation and dephosphorylation through kinases and phosphate-donor ATP respectively phosphatases and phosphate-acceptor ADP. Derived and modified from Ardito *et al.* 2017 [77] and created with BioRender.com.

The most common p-site is serine with more than 80%, followed by threonine with approximately 12%, and tyrosine (O-phosphorylation) with less than 2%, whereby phosphorylation of tyrosine residue is typical among EGFR family, containing a tyrosine kinase domain. A variety of biological processes (protein synthesis, proliferation, aging, differentiation, and apoptosis) are regulated through activation or inactivation of distinct enzymes and receptors by phosphorylation or dephosphorylation, as in the case of the p53 signaling pathway. Phosphorylation of p53 activates cell cycle control resulting in apoptosis, when required, and a dysfunction in proper phosphorylation may result in transformation into a cancer cell. Another prominent pathway is the MAPK/ERK, which is activated by a cascade of phosphorylations. Protein phosphorylations play a crucial role in a couple of cancer developments, and thus protein kinases serve as potential targets for anticancer drugs. [77] A well-known target in cancer treatment is PI3K, which is attributed to regulate several important physiological processes. [78]

Thus, the goal, the reason, and the analytical method of phospho-proteomics are evident, but due to high rate and dynamics of phosphorylation and dephosphorylation processes, proper analysis is quite challenging. [72, 79] Table 5 provides an overview of the limitations in phospho-proteomics summarized by Solari *et al.* 2015. [80]

Table 5 Limitations and difficulties in phospho-proteomic analysis.

1.	Analysis of low abundant proteins
2.	Low phosphorylation stoichiometry
3.	Potentially impaired digestion efficiency
4.	Loss of phosphopeptides during sample preparation and/or chromatography
5.	Impaired ionization efficiency of phosphopeptides
6.	Impaired identification of peptide sequence
7.	Impaired identification of correct localization of phosphorylation site(s)
8.	General limitations of peptide centric proteomics

Phosphorylation may interfere with enzymatic digestion of proteins through formation of salt bridges involving phosphoserine (pS) and phosphothreonine (pT), which in turn affects quantification. [81] The impaired identification of peptide sequence and correct localization of p-sites is attributed to bad quality of MS/MS spectra due to the special behavior of the labile phosphate group in collision-induced dissociation (CID). To ensure a maximal reproducibility, no changes in phosphorylation profiles, reduced samples losses, and no artificially introduced modifications, an accurate experimental setup is essential. Several serious problems arise during sample preparation (e.g., usage of agents potentially causing PTMs, such as non-freshly prepared urea or certain silver staining protocols) or already in the sample collection (e.g., operating too slowly). [80] The EasyPhos (EP) workflow minimizes such problems in sample preparation by eliminating protein precipitation and sample transfer steps, in turn increasing reproducibility and simultaneously reducing the required sample amount. [82]

To overcome the problem of low phosphorylation stoichiometry, specific enrichment techniques (applied upon peptide level) have been developed to identify phosphopeptides and thus phosphoproteins in a broad range. Quantitative phospho-proteomics is still challenging as the used strategies, such as

isobaric tags for relative and absolute quantification (iTRAQ) or stable isotope labeling by/with amino acids in cell culture (SILAC), require chemical or metabolic labeling of stable isotopes, and SILAC, for example, is not suitable for the analysis of clinical samples [80] Graaf *et al.* 2014 described a label-free method which is quite selective, sensitive and reproducible, namely titanium-immobilized metal ion affinity chromatography (Ti^{4+}-IMAC) based phosphopeptide enrichment. [83] Another commonly used enrichment strategy is the metal oxide affinity chromatography (MOAC), in which phosphopeptides are linked to metal oxides (e.g., TiO_2) via affinity binding of the phosphate group. Further enrichment methods available are inorganic salt affinity chromatography, co-precipitation, ion exchange chromatography, chemical derivatization, and immunoprecipitation. [84] A major advantage of MOAC involving TiO_2 is the high selectivity for phospho-peptides and the tolerance for widest range of reagents (buffers and salts) used in cell culture experimental procedures. [85] It was described in Hogrebe *et al.* 2018 that label-free quantification (LFQ) and SILAC methods provide higher accuracy, but tandem mass tag (TMT) methods yield better precision when performing quantitative phospho-analyses, and thus MS/MS-based TMT is recommended whenever achieving reproducible results is desired. For accurate but not necessarily reproducible quantifications, LFQ and/or SILAC methods with multiple replicate measurements should be preferred. [86]

1.3. Mass spectrometry

MS is the preferred technique for identification and characterization of proteins and their PTMs since the late 1990s. [60, 87] In MS/MS, identification of peptide fragments by alignment with a database results in improved accuracy of protein determination. [63] The principle of MS relies on the determination of the molecular weight by detecting the m/z of a molecule, and the first mass spectrometer was built by J.J. Thomson (with the help of Francis Aston) in 1912 and was a so called parabola spectrograph for analysis of positive rays. [88, 89] For years, MS was primarily used in the field of physics, until the 1940s when MS began to be used in industrial chemistry as a method for determining concentrations. [88] The introduction of fast atom bombardment (FAB) as an ionization method by Barber *et al.* 1981 [90] enabled fragmentation and thus identification of peptides using a neutral argon beam for ionization and was suitable for a mass range up to 12,000. [91] A breakthrough in MS was achieved by Comisarow and Marshall combining Fourier-transform (FT) with ion cyclotron resonance (ICR), resulting in FT-ICR MS. The principle of ICR, described first by J. A. Hipple in 1949, is to bring the particles into phase coherence by applying an oscillating electric field, and to obtain a complete spectrum, the magnetic field must be varied. Combination of ICR with FT allowed simultaneous measurement of all ions, and thus increased resolution while maintaining sensitivity. The revolution towards the ability to analyze large organic molecules, such as proteins, nucleic acids, or complex carbohydrates, via MS arose in the late 1980s with the introduction of the ESI and MALDI ionization techniques. [88] Prior to this, only smaller molecules, e.g. peptides, could be analyzed and relatively high concentrations were required for the analysis of smaller proteins. [88, 91]

ESI was actually inspired in the 1960s (1968 [92]), but was first implemented in the 1980s by spraying sample molecules in a solvent stream under atmospheric pressure using a potential difference of several thousand volts upstream of the mass analyzer. [93, 94] It can be coupled readily to HPLC and is usually

combined with triple quadrupole (QQQ) or IT mass analyzers. MALDI is a derivative of laser desorption, and laser desorption technique had already been used in the 1960s. [91] However, further improvement in sample preparation (embedding in a laser light-absorbing matrix) made it possible to use it as a soft ionization method, namely as MALDI, in the late 1980s. [95] MALDI is most commonly coupled to a TOF mass analyzer, in which the introduced ions are identified by measurement of their time needed to reach the detector. [91]

Beyond the above mentioned MALDI and ESI, there are other ionization sources commonly available, such as electron ionization (EI), chemical ionization (CI), atmospheric pressure chemical ionization (APCI), or atmospheric pressure photo ionization (APPI). [66, 94, 96]

Depending on the ionization technique applied, an appropriate sample preparation must be performed. Sticking to ESI and MALDI as examples, nebulization of the analyte in ESI requires accordingly liquid samples, while before MALDI the analyte is acidified and crystallized using a matrix, such as α-cyano-4-hydroxycinnamic acid and 2,5-dihydroxybenzoic acid or 3,5-dimethofy-4-hydroxycinnamic acid, thus becoming a solid sample. [91] An increased ionization efficiency in MALDI was achieved by using iTRAQ, resulting in improved identification of low abundant proteins in complex biological samples. [97] Alternatively, the identification of proteins in such samples can be enhanced by reducing the complexity of the sample prior to analysis as part of the sample preparation. [62] Both techniques can be coupled to upstream 2D-LC, resulting in the identification of different peptides due to their differences in ionization methodology. Note, that separation via LC is usually combined with ESI MS/MS. [62, 97] As the experimental procedures within this master's thesis employed an ESI as ionization source, the methodology is explained in more detail below.

As already pointed out, ESI uses a high potential while spraying the analyte, more precisely, several thousand volts are applied under atmospheric pressure to generate small, charged droplets. These droplets are forced to shrink by evaporation of the solvent, resulting in a convergence of the charges in the droplets, which in turn causes the repulsion of the charges to become greater than the surface tension of the droplets, leading to a coulomb explosion. Shrinking, charge repulsion, and coulomb explosion repeat until the obtained ions are small enough (compare Fig. 5), subsequently desolvated via inert gas (usually nitrogen), focused by a skimmer and delivered to the analyzer. With the temperature and flow rate, the efficiency of the ionization ca be controlled. For example, loss of sensitivity occurs when the flow rate is too high, as fewer mobile ions cannot be collected. If the flow rate is too low, too many ions may be solvated. This in turn could be preferable in special cases, e.g., when studying cluster properties, and can also be achieved by reducing the temperature. [94]

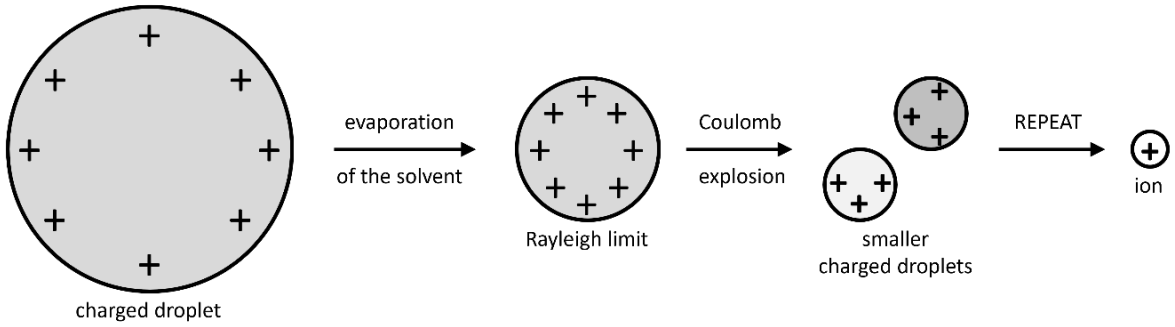

Figure 5 Scheme of the electrospray ionization principle showing the evaporation of the solvent, the Coulomb explosion, and the resulting ion. Derived and modified from Fenn *et al.* 1989. [94]

Talking about mass analyzers, it is necessary to always distinguish whether it is a MS or MS/MS, as the instrumental set-up differs. The major advantage of MS/MS compared to MS is the ability of identifying peptides in a complex biological sample without performing a thorough separation within sample preparation, and compared to chemical detection methods, post-translational modified peptides or proteins can be identified with MS/MS. By using an ESI-QQQ system as example, the difference between MS (normal scanning mode) and MS/MS can easily be explained or rather shown. In MS mode, the first (Q1) and second (Q2) filters are set to transmit, and the third (Q3) is used to scan over a defined mass range, thus detecting the ions passed respectively their masses. In contrast, the MS/MS mode works quite differently with Q1 filtering and only transmitting ions with a specific mass (all others are removed). In Q2, these ions are then fragmented by CID using a collision gas (normally argon at 1-4 mTorr), and the fragments are scanned in Q3 and thus analyzed. The collision energies are in the range of 10-40 eV and therefore only peptide bonds are broken, so fragmentation only occurs upon peptide bonds. At higher collision energies, side chains could be fragmented. Hence, MS/MS allows the determination of proteins based on the detection of specific peptide fragments of selected peptides, rather than just scanning and identifying present peptides as in MS. [91]

As mentioned previously, the most common mass analyzers are the Q, TOF, IT, and FT-ICR instruments, with the most used being combinations of them, such as QQQ, Q-TOF, Q-IT, or Q-ion mobility-TOF. [50, 88, 91] The principle of a TOF mass analyzer relies, as indicated by the name, on the time of flight, i.e., the velocity, of the ions in the ion channel until they make it to the detector. The ions are accelerated before entering the channel and the velocity is proportional to the accelerating voltage and the mass. An ion-gate at the beginning allows the selection of certain ions to pass through the channel, and these ions can decay due to collisional activation in the initial desorption cloud, and thus travel through the flight channel as daughter ions. Using a reflectron delays the time of flight of the individual ions, thereby improving the mass resolution, hence increasing the sensitivity and accuracy of the analyzer, with a mass range of over 500,000. [91]

Another commonly used mass analyzer is the Orbitrap, an IT instrument that has become more powerful by coupling with other mass analyzers, such as a Q, resulting in the QExactive™ series. [59] Other available instrumental set-ups of an Orbitrap are direct coupling to an ionization source, termed Exactive, or else coupling of a low resolution linear ion trap with the high resolution Orbitrap, resulting in a linear trap quadrupole (LTQ) Orbitrap. The difference of these instruments is reflected in their ability

to select ions, with no mass selection in the case of the Exactive. The LTQ Orbitrap selects ions in time (trap-trap), first isolating them, then fragmenting, and finally scanning the ions, and it is distinguished between CID and higher energy collisional dissociation (HCD). For CID, both analyzers work as separate mass spectrometers, whereas for HCD the linear ion trap is only used to isolate specific precursor ions and the Orbitrap performs scanning. In case of the QExactive setup, ions are selected in space (filter-trap), i.e., those ions having a stable trajectory due to their m/z range are selected and forwarded to the C-trap accordingly before being scanned by the Orbitrap. The C-trap is located between Q and Orbitrap, and is typically used for collection of the ions elected by the Q. In MS/MS analyses, the precursor ions are passed into the collision cell from the C-trap, and the obtained peptide fragments are finally scanned by the Orbitrap. [98] The fundamental mechanism of an Orbitrap mass analyzer is based on the spindle-shaped electrode in the middle around which the injected ions orbit, whereby the image current of the ions axial motion is measured, which is then converted into high-resolution mass spectra using FT. [99, 100] The first functioning devices were available in the early 2000s, owing to the development of a prototype by Makarov. [101, 102]

A quite recent development is trapped ion mobility spectrometry (TIMS)-MS, which is a hybrid of MS and ion mobility spectrometry (IMS) and is based on holding the ions stationary (trapped) in a flowing gas column by an electrical field (equal forces of gas flow and electric field), instead of the usual practice of chasing ions through a stationary gas, as is performed in IMS. Hence arises the spatial advantage of the method, namely a rather small analyzer with about 5 cm and a comparably large analytical gas flow column of up to 10 m. TIMS represents a promising alternative to ion mobility and features high resolving power, duty cycle, and efficiency, and furthermore, TIMS can be applied to a wide range due to its flexibility. Best example is the parallel accumulation serial fragmentation (PASEF) workflow, making TIMS-MS suitable for shotgun proteomics. [96] Hybridization of IMS with MS already achieves remarkable advantages, such as separation of geometric isomers, and by combining TIMS with MS, the scanning velocity and range of voltage (mobility) can be easily adjusted (speed vs. range vs. resolution), since the basis of separation in TIMS is due to the elution voltage. This ensures the high flexibility of TIMS in comparison to IMS. [103]

Michalski *et al.* 2011 demonstrated that only about one in six or seven of more than 100,000 eluted peptide species was accessible with LC-MS/MS. [104] Utilizing the above-mentioned PASEF method and coupling of TIMS and TOF, more than hundred MS/MS events per second can be acquired at full sensitivity. The increase in sequencing rate achieved by PASEF mode allow accurate quantification of more than 6,000 proteins in a single run, and online PASEF achieves remarkable sensitivity. PASEF combined with TIMS-TOF (as established on the Bruker timsTOF Pro) is a noteworthy high-sensitivity tool for proteomics. [105, 106] Even in the more challenging field of lipidomics, TIMS plays a highly sensitive role and enables in combination with PASEF the identification of more than three times as many lipids as with TIMS-MS/MS setup alone, thus increasing the sensitivity to the attomole range. [107]

Already in the 1990s, database searching methods in the field of proteomics were described in the context of peptide mass fingerprinting. The measured masses, or more precisely m/z ratios, of the peptides generated by digestion did not reveal which peptide/protein was present, but it was recognized that these masses were specific and by registering them in a database and further aligning them, the

proteins of interest could be identified. [91] The idea for protein identification via databases was already taken up in the early 1980s by Oliver *et al.* 1983. [108] Due to the rise of MS/MS fragment spectra, i.e., peptide fragment fingerprinting, the database entries were expanded and thus the database searches or rather the mode of searches were further developed, on top of that, algorithms were developed to automatically extract the spectra and by means of the precursor ion mass, the detected AA sequences were identified by matching with the database. This was in particular advantageous in that the numerous generated MS/MS spectra did not need to be evaluated manually. [91] It can thus be generally said that thanks to databases and the search algorithms, a vast number of proteins can be identified fast and accurately via MS. However, the quality of the results depends strongly on the generated spectra and thus the data to be interpreted, as well as on the used database. [50]

The currently most reliable respectively best-known protein databases available include UniProtKB (Universal Protein Knowledgebase), which is a collaboration between the European Bioinformatics Institute (EMBL-EBI), the Swiss Institute of Bioinformatics (SIB), and the Protein Information Resource (PIR), and thus evolved from the databases Swiss-Prot, TrEMBL, and the Protein Sequence Database (PIR-PSD) [73] and the National Center for Biotechnology Information (NCBI) database with the Basic Local Alignment Search Tool (BLAST) algorithm [109]. In the field of phospho-proteomics the PhosphoSitePlus® database [79] presently prevails on these days, along with UniProtKB [73] and PHOSIDA [75]. Other accessible databases, such as REACTOME [110], are used to visualize, analyze and interpret signaling pathways after successful protein identification.

2. Aim of the thesis and experimental layout

The goal of this thesis was to design a suitable experimental setup for an *in vitro* study in which the microenvironment of ovarian cancer is mimicked adequately to perform subsequent microscopic and proteomic investigations to trace potential alterations both morphologically and proteomically. For this purpose, two human epithelial ovarian adenocarcinoma cell lines, namely SKOV-3 and OVCAR-3, were used as models for hypoxia and shear stress experiments. The combination of microscopic and proteomic investigation arises from the treatments, as protein changes are expected in cells incubated under reduced oxygen (hypoxia) and morphological changes in cells subjected to biomechanical stimulation (shear stress). The two chosen cell lines represent different types of ovarian adenocarcinomas and thus different tumor spreading behavior: non-miliary (SKOV-3) and miliary (OVCAR-3).

Cells were seeded into 6-well plates for incubations (hypoxia, and shear stress) and were imaged (bright field and phase contrast) before and afterwards. Furthermore, two wells per plate of the plates for the hypoxia experiments (hypoxic and normoxic plate) were stained, see Fig. 6, to allow observation of mitochondrial changes during hypoxic exposure. The hypoxic plate was incubated in the Lionheart™ FX Automated Microscope connected to a computer with Gen5 Software Features for Imaging & Microscopy (BioTek Instruments, Winooski, VT, USA). Incubation in the Lionheart™ FX Automated Microscope allowed only one plate to be maintained under hypoxic condition, which was the limiting factor of the experimental setup. The impact of hypoxic and shear stress on the morphological and proteomic appearances of OC cells was examined.

The aim of this thesis was establishing the experimental setup and the initial evaluation of the impact of a low-oxygen environment (hypoxia) respectively biomechanical stimulation (fluid shear stress) on the morphology and proteome of two representative ovarian cancer cell lines.

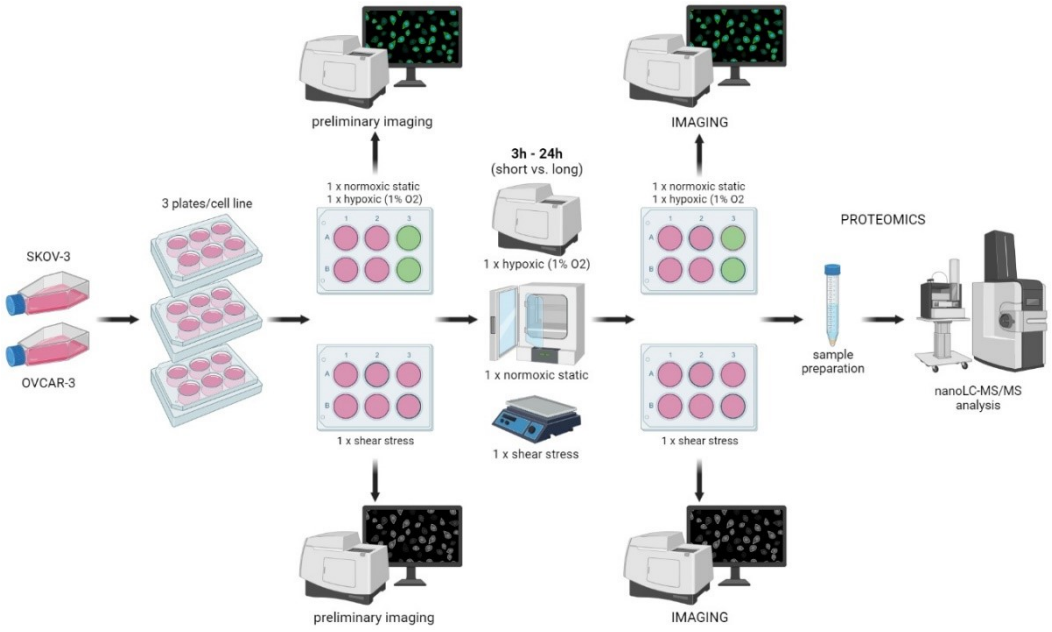

Figure 6 Experimental design of a complete hypoxia and shear stress experiment including normoxic static controls. Created with BioRender.com

3. Materials and Methods

3.1. Cell culture

The two human epithelial cell lines (SKOV-3 and OVCAR-3) used in the development of this thesis were both acquired from the American Type Culture Collection (ATCC, Manassas, Virginia, USA) and cultivated in the recommended base media supplemented with heat-inactivated fetal calf/bovine serum (FCS, Gibco, Thermo Fisher Scientific, Austria) and Penicillin-Streptomycin (P/S, Sigma-Aldrich, Austria) in humidified incubators (37 °C and 5% CO2). SKOV-3 cells were cultivated in McCoy's 5a Medium Modified (Gibco, Thermo Fisher Scientific, Austria) with 10% (v/v) FCS and 1% (v/v) P/S, and OVCAR-3 cells were cultivated in RPMI-1640 Medium (Gibco, Thermo Fisher Scientific, Austria) supplemented with 20% (v/v) FCS, 1% (v/v) P/S and 1% (w/v) insulin-transferrin-selenium (ITS-G, 100X, Gibco, Thermo Fisher Scientific). The cells were cultured in T25 cell culture flasks for adherent cells (Sarstedt, Austria) and splitted three times a week (every two to three days), as described in the following steps: first the medium was removed by pipette laterally from the flask in order to avoid harming viable cells. Cells were washed with 5mL room tempered Phosphate-Buffered Saline (PBS, Sigma-Aldrich, Austria), 2mL Trypsin-EDTA solution 0.25% (Sigma-Aldrich, Austria) were added to the cells and incubated for 8 minutes at 37 °C. Detached cells were rinsed with 3 mL complete medium, collected by pipette, transferred into a 15 mL Falcon tube and centrifuged at 220g (Heraeus™ Megafuge™ 16R, Thermo Scientific) for 5 minutes to remove Trypsin-EDTA by removing the supernatant. Cells were carefully re-suspended in the respective complete medium and seeded in a ratio of 1:2 or 1:3 in case of OVCAR-3 cells and 1:4 to 1:6 in case of SKOV-3 cells depending on cell density. Cells were regularly checked for mycoplasma contamination (MycoAlert™ Mycoplasma Detection Kit, Lonza).

3.1.1. Hypoxic exposure

For the experiments, cells were seeded into 6-well plates for adherent cells (Sarstedt, Austria) with 150,000 cells/well (SKOV-3) respectively 300,000 cells/well (OVCAR-3) in 2 mL completely supplemented medium per well. Cell counting was done with a MOXI Z Mini Automated Cell Counter with the corresponding MOXI Z Type M Cassettes (ORFLO Technologies, USA). After 24 hours setting time, cells showed confluence of about 80% and were prepared for the experiment according to the experimental layout as described above. The medium in the two wells to be stained of each plate was removed by pump and each of the respective wells was incubated with 1 mL staining solution (Hoechst 33258 and MitoTracker™ Green diluted 1:1000 in the respective base media) for 20 min in the dark. Afterwards the staining solution and the medium from the unstained wells were removed by pump, each well was washed with 1 mL PBS and then refilled with 2 mL of the appropriate completely supplemented medium. The 6-well plates were then either placed in the standard incubator (normoxic control) or in the Lionheart™ (hypoxic exposure) and were incubated for 24 hours (Proteome Profiling) or 3 hours (Phospho-Profiling) under the corresponding oxygen condition (37°C, 5% CO_2, 20% O_2 and 75% N_2 respectively 1% O_2 and 94% N_2). Hypoxia in the Lionheart™ was achieved with the CO_2/O_2 gas controller from BioTek by flushing the system with N_2.

3.1.2. Shear stress

Cells were prepared identically as for the hypoxia experiments with 150,000 cells/well (SKOV-3) respectively 300,000 cells/well (OVCAR-3) in 6-well plates, each well with 2 mL of appropriate completely supplemented medium. After a setting time of 24 hours, fresh medium was added to the cells shortly before the experiments. As no fluorescence imaging was performed as part of the shear stress experiments, there was no preliminary staining. The control plates were then normally placed in the standard incubator (static control), whereas the plate subjected to shear stress was put in the orbital shaker (IKA MS 3 basic shaker, Germany) which was placed in the standard incubator. All plates were then incubated for 24 hours (long-term) or 3 hours (short-term) under normal oxygen conditions (37°C, 5% CO_2, 20% O_2 and 75% N_2). Shear Stress τ_w of about 2.8 dyne/cm² was achieved with the orbital shaker method, as described in Warboys *et al.* 2019 [111], by adjusting the speed to 250 rpm (= 26.1799 rad/s).

Equation 1 Calculation of the shear stress τ_w in dyne/cm² with a = radius of rotation of the shaker in cm, ρ = density of the medium assumed as 1 g/cm³, μ = dynamic viscosity in dynes/cm², and ω = angular velocity in rad/s.

$$\tau_w = a\sqrt{(\rho\mu\omega^3)}$$

$$250\ rpm: \quad \frac{?\ dyne}{cm^2} = 0.225\ cm \cdot \sqrt{\frac{1\ g}{cm^3} \cdot \frac{8.9 \cdot 10^{-3}\ dyne \cdot s}{cm^2} \cdot \left(26.1799 \frac{rad}{s}\right)^3} = 2.8434 \frac{dyne}{cm^2}$$

3.1.3. Live cell imaging and image analysis

Prior and after the appropriate incubation, all 6-well plates were imaged with the Lionheart™ with at least 4 center optical fields per well using Gen5 Software Feature for Imaging & Microscopy. The hypoxic plate, incubated in the Lionheart™ itself, was additionally imaged automatically at least once per hour during the incubation period. For every plate, bright field and phase contrast images were acquired from the central area of each well, as well as fluorescence images of the stained wells (10X magnification). Image analysis was performed with Gen5 software (fluorescence images) and with the free software ImageJ (phase contrast images, morphological analysis, see Fig. 7).

For the morphological analysis of phase contrast images, at least 5 representative cells per image were evaluated in terms of area, perimeter, major and minor axis, circularity, and roundness. For this purpose, the scale in the software (Analyze, Set Scale…) for the respective image batch was first set in relation to the scale indicated by the Lionheart™ on the images. Furthermore, the parameters to be measured were defined (Analyze, Set Measurements…), namely area, center of mass, perimeter, and fit ellipse, and in addition “Display label” was selected. Then the outlines of the selected representative cells were traced and measured (ctrl+M) using the “Freehand selections” tool. The obtained data were inserted into previously prepared evaluation sheets.

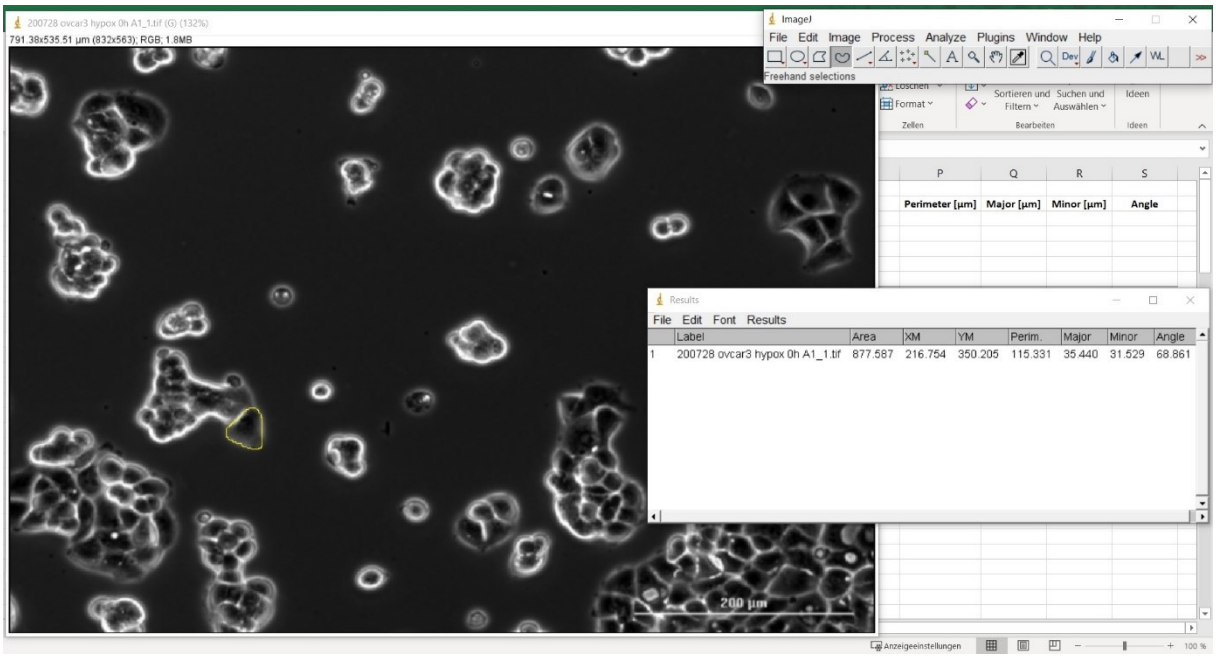

Figure 7 Screenshot of image analysis with ImageJ. An exemplary image of the OVCAR-3 cells, with a representative cell selected of which the area, perimeter, and major and minor axis were calculated by the software.

For analysis of the fluorescence images with the Gen5 software, the images acquired before and after the incubations were evaluated with respect to cell count and nuclei area in case of Hoechst staining, whereas the Mito sum area and Mito sum integral were evaluated in case of MitoTracker™ Green staining. Therefore, a corresponding image was displayed in the respective channel (DAPI for Hoechst or GFP for MitoTracker™ Green) and with the image analysis tool (Analyze…) the parameters shown in table 6 were set. Finally, the above mentioned metrics (cell count and nuclei area for DAPI channel, Mito sum area and Mito sum integral for GFP channel) were calculated and the obtained data were exported to an Excel sheet.

Table 6 Parameters for Image Analysis with Gen5 Software.

	SKOV-3		OVCAR-3	
channel	DAPI	GFP	DAPI	GFP
Threshold Value	10,000	4,000	5,000	3,500
Min. cell size	5 µm	5 µm	5 µm	5 µm
Max. cell size	40 µm	500 µm	40 µm	500 µm
Primary edge objects included	Yes	Yes	Yes	Yes
Rolling Ball	30 µm	300 µm	10 µm	400 µm

3.1.4. Cell lysis

The 6-well plates were immediately after imaging placed on ice and the cells of the unstained wells were processed, consequently on ice, for the corresponding MS analysis (Proteome or Phospho-Profiling) as described below.

For Proteome Profiling, the SOP Cell fractionation protocol was applied with the crucial steps as follows. The medium of the unstained wells was removed by pipette and discarded, cells were washed two times with 2 mL ice-cold PBS and treated with 1 mL fractionation buffer (10 mM HEPES/NaOH (pH = 7.4), 10

mM NaCl, 3.5 mM $MgCl_2$, 1mM Ethylene glycol-bis(aminoethyl ether)tetraacetic acid (EGTA), 250 mM sucrose, 0.5% Triton X-100), supplemented shortly before fractionation with Protease and Phosphatase Inhibitor Cocktail (PPC, Sigma-Aldrich, Austria) and phenylmethylsulfonyl fluoride (PMSF, Sigma-Aldrich, Austria, 1.742 g in 100 mL isopropanol). Cells were scraped off the wells with a cell-scraper (using the same scraper for biological replicates) and the cell suspension was then transferred with a syringe and needle (1 mL syringe and short needle, using the same ones for biological replicates) to a falcon tube, where cells were lysed with shear stress by pipetting the suspension up and down and pressing against the wall of the falcon tube 10 times. To control if cells were lysed, an aliquot was checked under the microscope. Cell suspensions were centrifuged at 2227g for 5 min at 4 °C and supernatants (containing cytoplasmic fraction, CYT) were transferred into prepared falcon tubes with 4 mL ice cold ethanol (EtOH, abs. 99%, AustroAlco, Austria) respectively. Falcon tubes were sealed with parafilm and stored at -20 °C in a labelled bag with the top up. The pellet (with nuclear fraction, NE) remained in the falcon tube was dried with tissue paper (abbussln) to remove residual CYT and was then dissolved in 100 µL TE-NaCl (10 mM Tris/HCl, 1 mM EDTA, 500 mM NaCl) by pipetting up and down. After incubating for 10 minutes on ice, 900 µL of prepared TE-NP-40-mix (10 mM Tris/HCl, 1 mM EDTA, 0.5% (v/v) nonidet P-40 (NP-40)) was added to each sample, shortly vortexed, incubated on ice for 15 minutes and then centrifuged at 2227g for 5 min at 4 °C. Supernatants (containing NE) were transferred into prepared falcon tubes each containing 4 mL ice cold EtOH, falcon tubes were sealed with parafilm and stored at -20 °C upside down in a labelled bag.

For Phospho-Profiling, a whole cell lysis was performed according to the steps described hereafter. Medium of every well was removed, each well was washed twice with 2 mL ice-cold PBS and then 100 µL of precooled (4 °C) SDC lysis buffer (4% (w/v) SDC, 100 mM Tris/HCl, pH = 8.8, prepared shortly before use) were added to the cells of each well. Cells were scraped down with a cell-scraper, cell suspensions of each column were pooled to one sample (thus 3 samples per plate were obtained) and transferred into 15 mL falcon tubes. Samples were heat treated in a water bath at 95°C for 5 minutes, after cooling to room temperature (RT) samples were homogenized by ultrasonic and then stored overnight at 4°C.

3.2. Sample preparation

Cytoplasmic and nuclear fractions of Proteome Profiling samples, stored at -20 °C, were sorted pairwise by weight and then centrifuged at 4536g for 30 min at 4 °C. After removing and discarding the supernatants, pellets were left to dry for 20 minutes by putting falcon tubes top down on tissue paper, followed by 30 minutes drying under vacuum (falcon tubes top up and turned away from vacuum). The dried pellets were then dissolved overnight in Protifi® lysis buffer (8 M urea, 50 mM TEAB, 5% (v/v) SDS, pH = 7.55), whereby the CYT were dissolved in 50 µL and the NE in 25 µL. Dissolved proteome profiling samples were transferred into previously labeled Eppendorf tubes, a BCA (bicinchoninic acid) assay was done to determine the protein concentration, and then the samples were stored in the freezer at -20 °C until further processing.

Phospho samples, stored overnight at 4°C in falcon tubes, were centrifuged at 700g for 10 minutes, supernatants were transferred into Eppendorf tubes and centrifuged (Eppendorf™ Microcentrifuge

5425) at 13,000g for 5 minutes. Supernatants were transferred into new pre-labeled Eppendorf tubes, then protein concentration was determined by BCA assay and the samples were stored in the freezer at -20 °C.

3.2.1. BCA assay

For determination of protein concentration, 6 calibration standards with 0-5 µL BSA (1 µg/µL) were prepared in Eppendorf tubes with respectively 9-4 µL LC-MS grade water, 1 µL lysis buffer (LB, Protifi® or SDC) and 200 µL working reagent. The working reagent was prepared directly before usage by mixing reagent A (26 mM bicinchoninic acid disodium salt hydrate, 186 mM sodium carbonate, 8 mM sodium tartrate, 113 mM sodium bicarbonate, pH = 11.25) and reagent B (200 mM copper sulfate pentahydrate) in a ratio of 50:1. Samples were also prepared in Eppendorf tubes by pipetting 1 µL sample, 9 µL LC-MS grade water and 200 µL working reagent. The tubes were incubated for 30 minutes at 60 °C in the dark with shaking at 1,100 rpm using the Thermomixer (Eppendorf™ Thermomixer™). After incubation, samples were briefly spinned off, then 200 µL each were pipetted into a 96-well plate and absorbance was measured at 562 nm without lid using the plate reader (Multiskan™ GO Microplate Spectrophotometer, Thermo Scientific™).

3.3. Proteomics

The proteins dissolved in LB (Protifi® or SDC) were then further processed according to the respective protocol. Proteome profiling samples from the 24 hour incubations, dissolved in Protifi® lysis buffer, were digested according to the Protifi® S-Trap™ protocol for micro columns. In contrast, phospho samples from the 3 hour incubations dissolved in SDC lysis buffer were processed using the in solution protein digestion, followed by the EP StageTip Phosphopeptide enrichment protocol.

3.3.1. Protifi® S-Trap™ micro digestion

Samples of the long-term experiments were diluted to 20 µg protein in a final volume of 25 µL Protifi® LB in Eppendorf tubes and then reduced by adding 25 µL DTT (64 mM) and incubating for 10 minutes at 95 °C at 300 rpm with the Thermomixer. After samples were cooled to RT and briefly spinned off, 6.25 µL IAA (486 mM) were added and incubated for 30 minutes at 30 °C in the dark at 300 rpm on the Thermomixer to alkylate cysteines. Again, the samples were briefly spinned off and then acidified with 5.63 µL 12% (v/v) ortho-phosphoric acid. To change buffer condition, 370 µL S-Trap™ buffer (90% (v/v) MeOH, 100 mM TEAB, pH = 7.1) were added, then 150 µL of the lysates were transferred to Protifi® S-Trap™ micro columns, which were placed into 2 mL Eppendorf tubes and centrifuged at 4,000g for 1 minute. Loading lysates on columns and centrifugation were repeated two times, followed by washing 4 times with 150 µL S-Trap™ buffer. The columns were rotated 180° between each centrifugation step and after every second centrifugation the Eppendorf tubes were emptied. Columns were transferred into new pre-labeled Eppendorf tubes and 20 µL Trypsin/LysC (20 µg Trypsin/LysC (Promega) immediately before use dissolved in 800 µL ice cold 50 mM TEAB, kept on ice) were added to each column, lids were closed and incubated for 2 hours at 37 °C in an incubator (Heratherm™ Compact Incubator, Thermo Scientific™) to allow digestion of proteins. Subsequently, the peptides were eluted by adding 40 µL digestion buffer (50 mM TEAB) to the digestion solution and centrifugation at 4,000g for 1 minute.

Elution was continued with addition of 40 µL 0.2% (v/v) formic acid (FA), centrifugation at 4,000g for 1 minute and finally the addition of 35 µL 50% (v/v) acetonitrile (ACN), 0.2% (v/v) FA and a last centrifugation step (4,000g for 1 minute). Peptides were dried at 40 °C using a vacuum concentrator (miVac Duo, Genevac™) and then stored at -20 °C in a labelled bag until further processing.

3.3.2. In solution protein digestion

The protein samples of the short-term experiments were diluted to a total protein amount of 200 µg in 270 µL SDC LB, 30 µL reduction/alkylation buffer (100 mM TCEP, 400 mM 2-CAM, pH = 7-8 with 5 M NaOH) were added to each sample and incubated in the dark at 45 °C for 5 min, shaking at 1,400 rpm using the Thermomixer. Samples were briefly spinned off and allowed to cool to RT. For protein digestion, 2 µL ice cold Trypsin/LysC (1µg/µL, 20 µg Trypsin/LysC were dissolved shortly before use in 20 µL trypsin buffer (0.05% (v/v) acetic acid, 2 mM $CaCl_2$), kept on ice) were added to each sample and incubated at 37 °C and 1,400 rpm on the Thermomixer overnight.

3.3.3. Phosphopeptide enrichment

400 µL isopropanol were added to each peptide sample and then shaken for 30 seconds at 1,400 rpm on the Thermomixer. Further, 100 µL EP enrichment buffer (48% (v/v) trifluoroacetic acid (TFA), 8 mM KH_2PO_4) were added and shaken again for 30 seconds at 1,400 rpm on the Thermomixer. In case of any precipitation, the samples were purified by centrifugation at 10,000g for 5 minutes at RT and subsequent transfer of the supernatant into new Eppendorf tubes. Titansphere™ TiO_2 beads (GL Sciences) were prepared by re-suspension in EP loading buffer (6% (v/v) TFA, 80% (v/v) ACN) at a concentration of 1 mg/µL and 3µL of the TiO_2 bead solution were added to each sample and incubated for 5 min at 40 °C and 1,400 rpm on the Thermomixer. The samples were then centrifuged for 1 minute at 2,000g and RT to pelletize the beads, followed by removal and discarding of the non-phosphopeptide supernatant. 1 mL of EP wash buffer (5% (v/v) TFA, 60% (v/v) isopropanol) was added to each sample, briefly vortexed (Vortex-Genie® 2) and incubated for 30 seconds at 1,400g and RT (Thermomixer). TiO_2 beads were again pelletized by centrifugation for 30 seconds at 2,000g, then the supernatant was removed and discarded. This washing step was performed five times in total (i.e., repeated four times). After washing steps, the TiO_2 beads of each sample were re-suspended in 75 µL EP transfer buffer (0.1% (v/v) TFA, 60% (v/v) isopropanol) and transferred to the top of a C_8-StageTip placed in an Eppendorf tube. In order to capture any remaining TiO_2 beads, another 75 µL EP transfer buffer was added to the sample tube and transferred to the respective StageTip. The StageTips were then centrifuged for 4 minutes at 1,500g, the passed through buffer was discarded and in case any TiO_2 beads remained in the sample tubes, another 75 µL EP transfer buffer were added to the tube, transferred to the respective StageTip and centrifuged again. Furthermore, the StageTips were placed in glass vial inlets in new 2 mL Eppendorf tubes and the phosphopeptides were eluted with 30 µL EP elution buffer (40% (v/v) ACN, 25% (w/v) ammonium hydroxide) and centrifugation for 5 min at 1,500g and RT. StageTips were rotated 180° and the elution step was repeated into the same glass vial inlet. Finally, the phosphopeptide samples were dried at 40 °C using a vacuum concentrator and the glass vial inlets were stored in the 2 mL Eppendorf tubes at -20 °C in a labelled bag.

3.3.4. Nano LC-MS/MS

Peptides of the Proteome Profiling samples were re-suspended in 5 µL 30% (v/v) FA, diluted with 40 µL mobile phase A (97.9% (v/v) H_2O, 2% (v/v) ACN, 0.1% (v/v) FA), and transferred into sample vials. Phosphopeptide enriched samples were re-suspended in 15 µL MS loading buffer (97,7% (v/v) H_2O, 2% (v/v) ACN, 0.3% (v/v) TFA) by ultrasonication for 5 minutes at 20% power, followed by centrifugation for 7 minutes at 5,000g. Afterwards, the glass vial inlets were transferred into glass vials and the samples were sealed with injection lids. 5-10 µL were injected into a Dionex 3000 nanoRSLC system with a C18 trapping column (2 cm × 100 µm, 3 µM particle size, C18, Thermo Fisher Scientific) and a subsequent C18 analytical column (50 cm × 75 µm, 2.6 µM particle size, C18, Thermo Fisher Scientific). The injected samples were separated by elution from the pre-column to the analytical column using a flow rate of 400 nL/min with a gradient of 8-40% mobile phase B (80% ACN, 20% H_2O, 0.1% FA) for 95 minutes. Thus, a total LC run time of 135 minutes including washing and equilibration steps was achieved.

For the MS analyses, the timsTOF™ Pro mass spectrometer (Bruker Daltonics Inc., Billerica, MA, USA) coupled to an ESI source (CaptiveSpray™, operating at 1,600 V) was used. The timsTOF™ has been run with the PASEF mode. Trapped ion mobility separation was done by using a $1/K_0$ scan range from 0.6-1.6 Vs/cm^2, leading to a ramp time of 166 milliseconds and each cycle was performed with 10 PASEF MS/MS scans, resulting in an overall cycle time of 1.88 seconds. The MS and MS/MS spectra were acquired with a scan range from 100-1,700 m/z, and the collision energy was increased from 20 to 52 eV as a function of increasing ion mobility. The full width at half maximum height (FWHM) Δm was set to 2 Thomson (Th) for m/z < 700, and to 3 Th for m/z > 700.

3.3.5. Data processing and analysis

The obtained raw data of proteome profiling and phosphoproteome experiments were analyzed with the freeware MaxQuant (version 1.6.17.0), which uses the Andromeda search engine. Then a statistical analysis was performed with the software Perseus (version 1.6.6.0). [112]

For a valid protein identification, a MaxQuant search against the human protein database UniProtKB (version 12/2019, reviewed entries only) [73] was performed with at least two peptide identifications, whereby at least one had to be a unique peptide. The digestion mode was defined as “specific”, namely Trypsin/P, with a maximum of two missed cleavages. Moreover, carbamidomethylation was set as a fixed protein modification, whereas oxidation of methionine, acetylation of the protein N-terminus, and phosphorylation of serine, threonine and tyrosine were set as variable modifications, and maximum two modifications per peptide were allowed. The false discovery rate (FDR) was set to < 0.01 for both peptide and protein level.

The obtained LFQ data were then further processed using the Perseus software, filtering, and removing potential contaminants, reversed sequences and proteins only identified by site. LFQ values were transformed, namely logarithmized to base 2, then grouped and averaged according to their replicates. Filtering based on valid values with the requirement to have at least 70% within a group was performed to remove invalid values. Furthermore, the missing LFQ values were replaced using a normal distribution with a down shift of 1.8 and a width of 0.3. Principal component analysis (PCA) and Volcano plots (FDR

< 0.05, S0 = 0.1, except for hypoxia data of OVCAR-3, where a S0 = 0.5 was selected) were created to identify significantly regulated proteins when compared to the respective treatment control (normoxia/static).

Further analysis and interpretation of the phosphopeptide data was performed by Patricia Bortel and Lukas Janker using PhosphoSitePlus and NetworKIN as described in Bileck *et al.* 2021. The analysis resulted in diverse graphs and waterfall plots of enriched kinases, and the findings and interpretations can be found in the corresponding article.

4. Results

Both ovarian adenocarcinoma cell lines (SKOV-3 and OVCAR-3) proliferate under the artificial hypoxic condition in the Lionheart™, as evident from the cell counts in Fig. 8. Similarly, proliferation of both cell lines is observed under shear stress using the orbital shaker method (see Supplementary Fig. S1). However, after 24 h incubation under both hypoxia and shear stress, cell counts for SKOV-3 are comparable to those of the controls (normoxia and static, accordingly), while cell counts for OVCAR-3 are visibly lower in comparison to the respective controls.

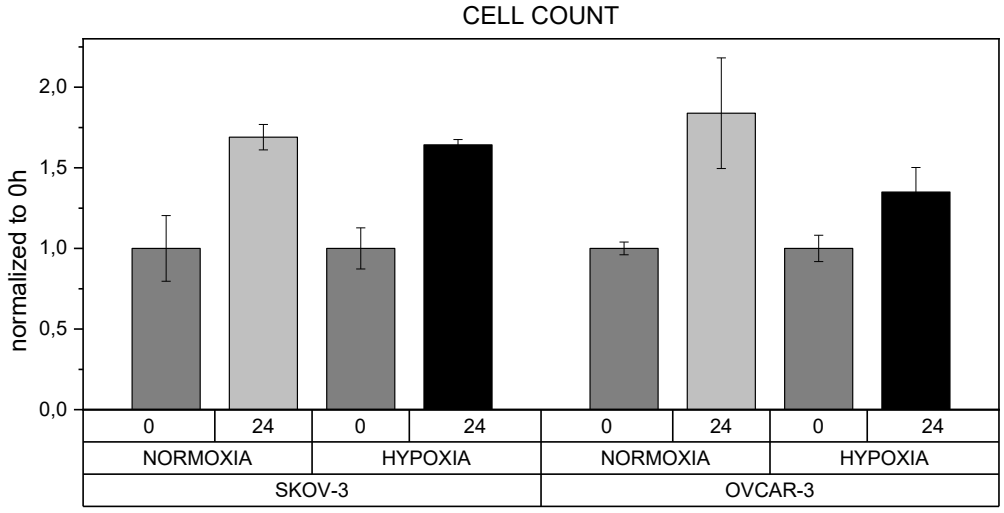

Figure 8 Results of cell counts of the image analysis with Gen5 Software of the fluorescence images, given as mean ± SD. Data are the results of n = 8 optical fields evaluated for both time points of each treatment per cell line. No significances indicated since the means ± SD are from n = 2 independent cell counts.

Moreover, both cell lines show protein regulations in each condition, with basically different significant regulations in the respective samples of CYT and NE fractions for both cell lines, except for the NE fractions of shear stress experiments, which show 48 common regulated proteins of the two cell lines.

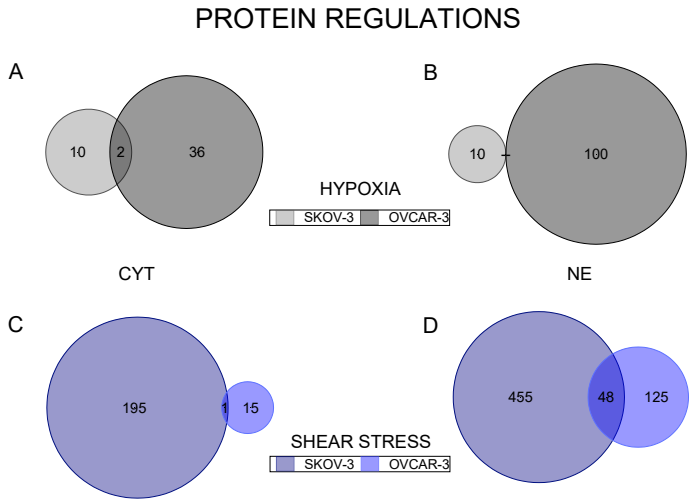

Figure 9 Venn diagrams of significantly regulated proteins of cytoplasmic (CYT, A and C) and nuclear extract (NE, B and D) of hypoxia (grey) and shear stress (blue) experiments. Numbers in circles indicate the numbers of regulated proteins.

4.1. Image analysis

All images (phase contrast and fluorescence) were acquired using the Lionheart™ FX Automated Microscope and analyzed as described in section 3.1.3 using the free software ImageJ and Gen5 Software, respectively.

4.1.1. Cell morphology

As already demonstrated by cell counts (Fig. 8 and Fig. S1) and obvious from the phase contrast images, both cell lines (SKOV-3 and OVCAR-3) proliferate well under both hypoxia and shear stress, compare Figs. 10 to 13.

SKOV-3 cells showed an increase in all evaluated parameters, except for roundness, after 24 h incubation under hypoxic condition, whereas shear stress decreased the size of SKOV-3 cells but increased roundness, each compared with the corresponding control.

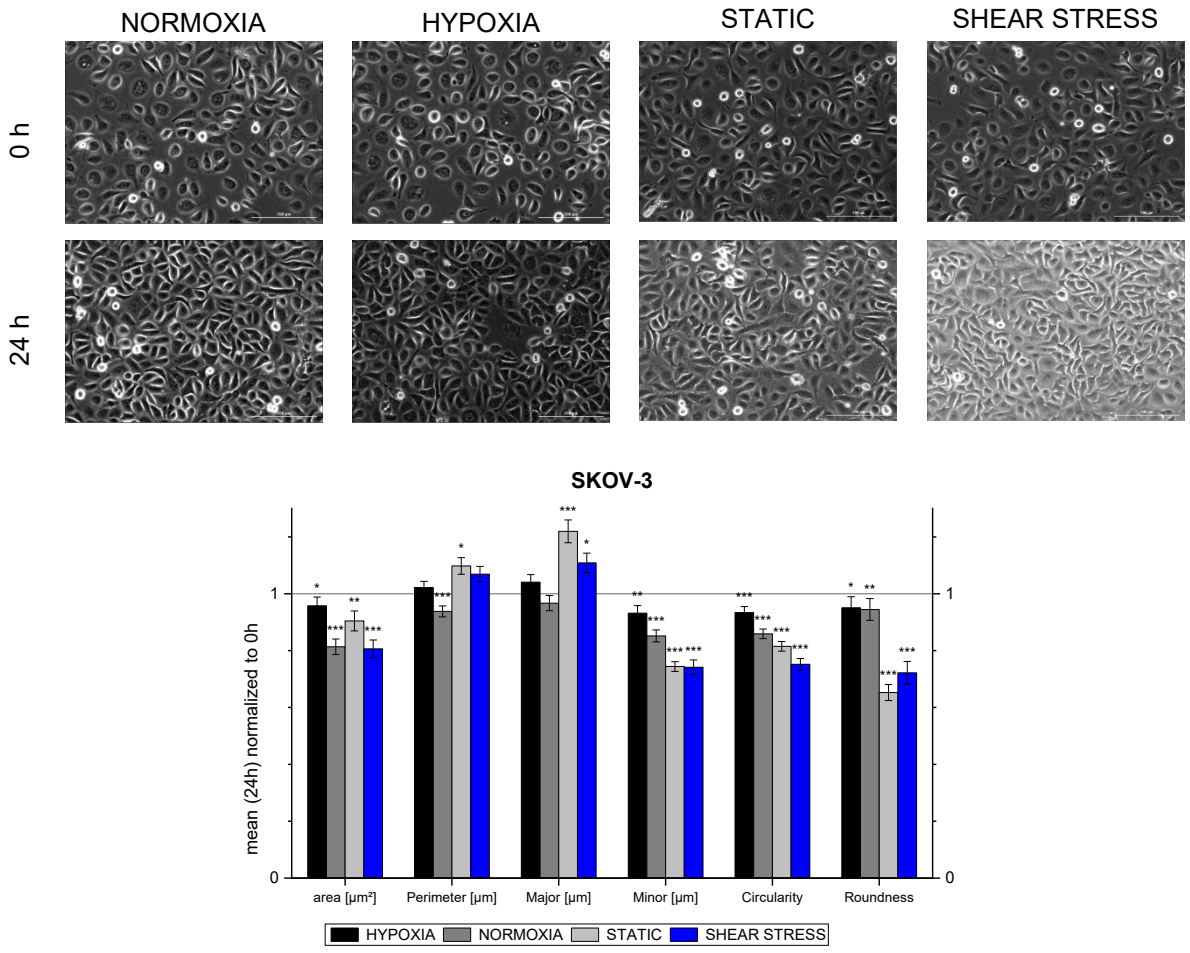

Figure 10 Representative phase contrast images of SKOV-3 cells before and after 24 h incubations (top). Results of morphological analysis with ImageJ software in respect to area, perimeter, major and minor axes, circularity, and roundness (bottom). Data given as mean ± SD are the results of n ≥ 60 evaluated cells per condition. Asterisk (*) indicates significant difference in comparison to 0 h, calculated with the t-test (*p < 0.05; **p < 0.01; ***p < 0.001).

After 3 h of hypoxia, neither significant differences compared to before incubation, nor to the treatment control (normoxic static) could be determined for SKOV-3 cells. In contrast, significant changes (indicated by asterisks) in morphology could be determined for SKOV-3 cells after 3 h of shear stress compared to before incubation, but no visible differences were observed with respect to the treatment control (normoxic static).

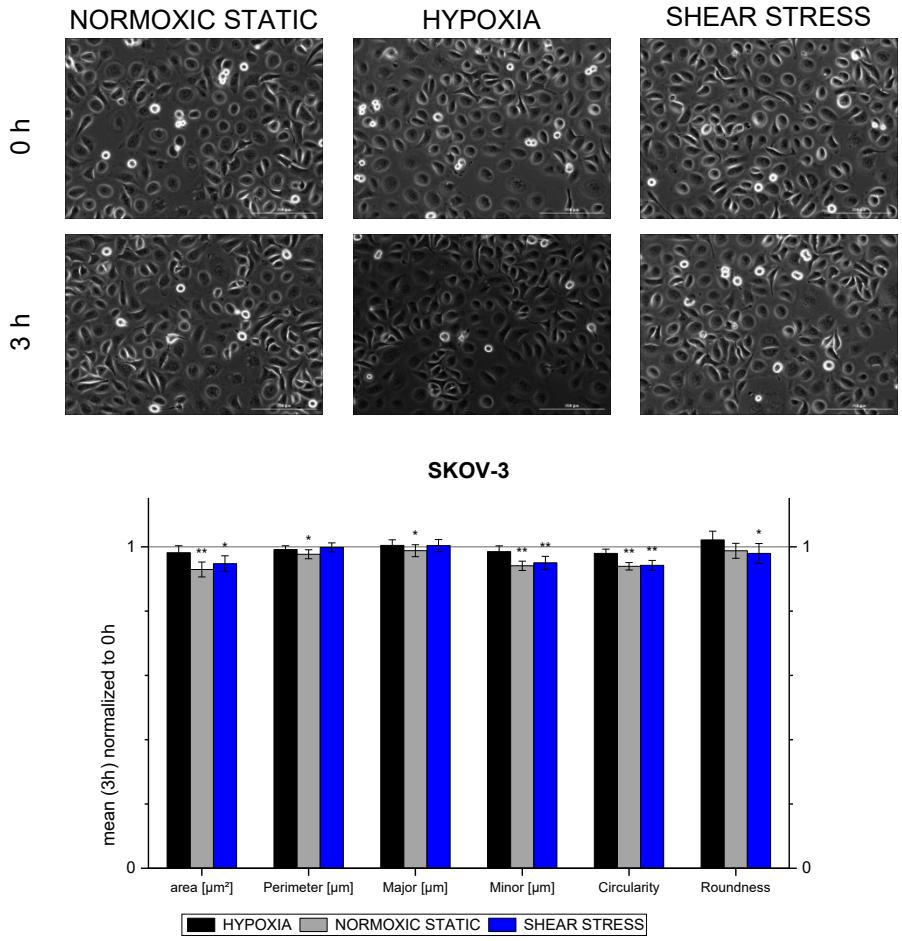

Figure 11 Representative phase contrast images of SKOV-3 cells before and after 3 h incubations (top). Results of morphological analysis with ImageJ software in respect to area, perimeter, major and minor axes, circularity, and roundness (bottom). Data given as mean ± SD are the results of n = 120 evaluated cells per condition. Asterisk (*) indicates significant difference in comparison to 0 h, calculated with the t-test (*$p < 0.05$; **$p < 0.01$).

OVCAR-3 cells increased size (indicated by area, perimeter, major and minor axes) but decreased roundness in both hypoxia and shear stress after 24 h treatment. The most prominent change (increase) compared to the respective control was observed for the area of OVCAR-3 cells after exposure to shear stress for 24 h (see Fig. 12 bottom).

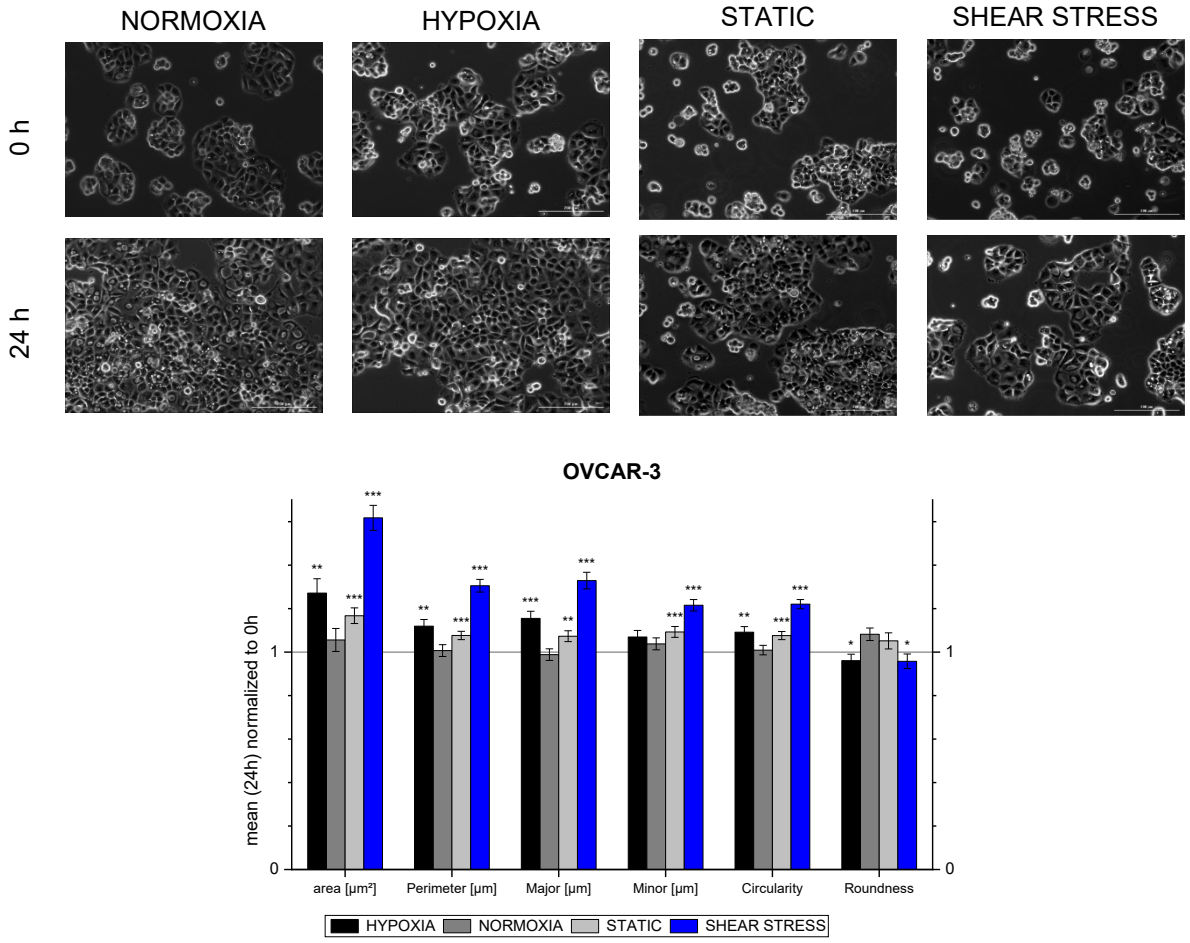

Figure 12 Representative phase contrast images of OVCAR-3 cells before and after 24 h incubations (top). Results of morphological analysis with ImageJ software in respect to area, perimeter, major and minor axes, circularity, and roundness (bottom). Data given as mean ± SD are the results of n ≥ 50 evaluated cells per condition. Asterisk (*) indicates significant difference in comparison to 0 h, calculated with the t-test (*p < 0.05; **p < 0.01; ***p < 0.001).

Already after 3 h hypoxia, OVCAR-3 cells showed obvious changes in size compared to 0 h and to treatment control (normoxic static). Under shear stress, OVCAR-3 cells also showed significant changes after 3 h treatment compared with 0 h (indicated by asterisks), but no distinct differences in comparison to the treatment control.

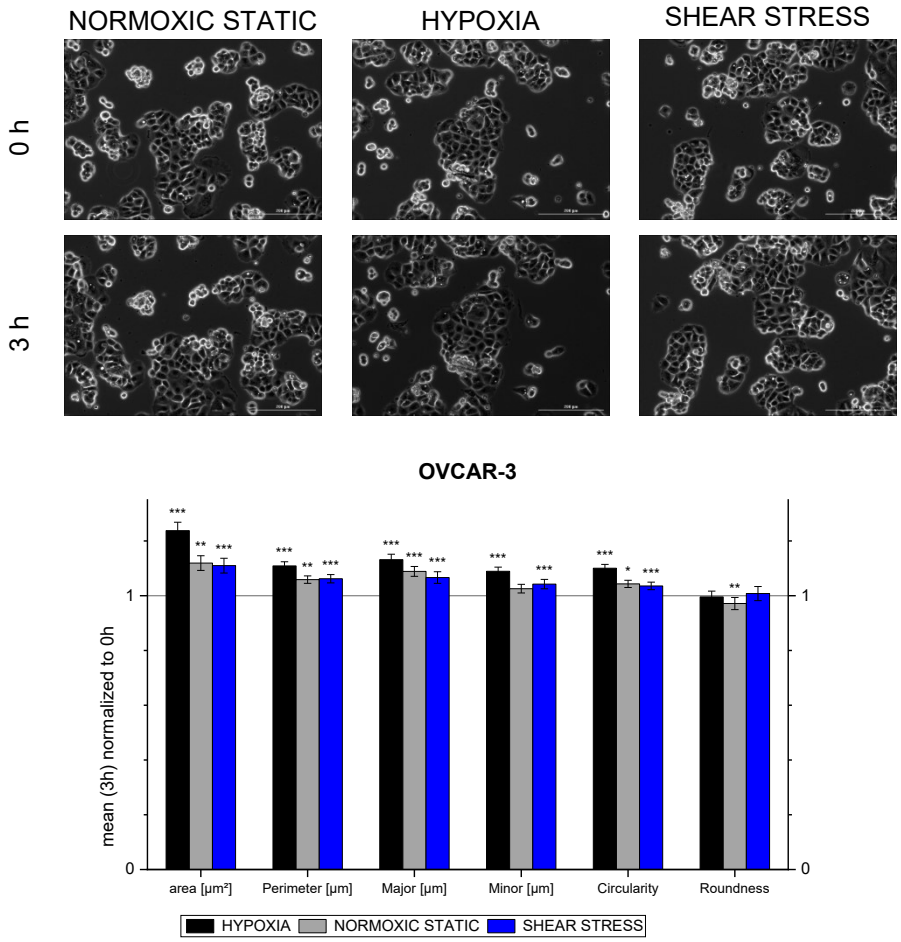

Figure 13 Representative phase contrast images of OVAR-3 cells before and after 3 h incubations (top). Results of morphological analysis with ImageJ software in respect to area, perimeter, major and minor axes, circularity, and roundness (bottom). Data given as mean ± SD are the results of n = 120 evaluated cells per condition. Asterisk (*) indicates significant difference in comparison to 0 h, calculated with the t-test (*p < 0.05; **p < 0.01; ***p < 0.001).

Morphological analysis revealed that both cell lines respond with changes in morphology to the applied stimulations. While both display similar morphological responses upon hypoxia, the appearance of the cells upon shear stress differs visibly. SKOV-3 decrease in size and increase in roundness, whereas OVCAR-3 clearly increase in size and decrease in roundness. Thus, these two cell lines behave completely contrary to each other in terms of their morphological adaption under shear stress. But under hypoxia, both cell lines increase their size and consequently their surface area.

4.1.2. Fluorescence analysis

Fig. 14 and S1 show representative fluorescence images of SKOV-3 (A) and OVCAR-3 (B) cells with the corresponding results of fluorescence analysis in terms of cell count, nuclei area, Mito sum area and Mito sum integral. As already mentioned, cell counts for SKOV-3 are comparable to those of the controls, whereas cell counts for OVCAR-3 are visibly lower in both conditions when compared to the respective controls. Upon hypoxia, the mean nuclei area increases for both cell lines, whereas the Mito area remains unchanged in SKOV-3 and increases in OVCAR-3. For SKOV-3 the mean integrated Mito fluorescence decreases but for OVCAR-3 visibly increases. The fluorescence images of the shear stress treatments emerged as part of the experimental setup and are therefore shown in the supplementary material and are weighted less for the conclusions. For both cell lines, little changes in Mito area and integrated fluorescence are seen after 24 h of shear stress, but both showing visible changes in static controls. The nuclei area of OVCAR-3 seems to be comparable for both shear stress and static, whereas the nuclei area of SKOV-3 behaves contrary under shear stress compared to static control.

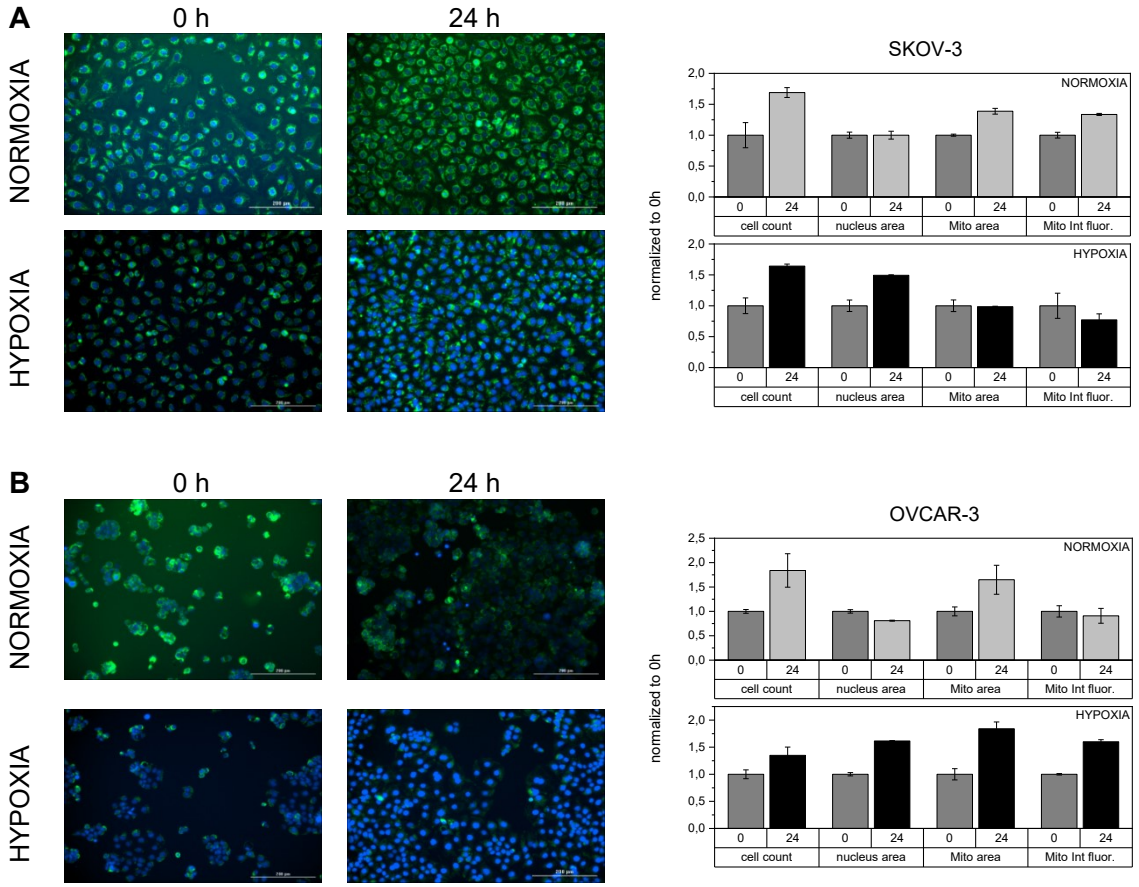

Figure 14 Representative fluorescence images (nuclei in blue, Hoechst, and mitochondria in green, MitoTracker™) of SKOV-3 (A) and OVCAR-3 (B) before and after 24 h hypoxic treatment with the corresponding results of fluorescence analyses acquired with Gen5 software. Data given as mean ± SD are the results of n = 8 optical fields evaluated for both time points of each treatment per cell line. No significances indicated since the means ± SD are from n = 2 independent cell counts.

Fluorescence analysis revealed different behavior of mitochondria of the two cell lines under hypoxic condition.

4.2. Proteomic analysis

Proteomic analysis, precisely proteome profiling and phospho profiling, revealed a range of protein regulations in both cell lines for hypoxic as well as for biomechanically stimulated cells. As described in section 3.3.5. (Data processing and analysis), the obtained MS data were first searched against the human protein database UniProt with the freeware MaxQuant and the LFQ data were further processed using the free software Perseus. After filtering and removing, logarithmizing, grouping, and filtering for valid values, the PCAs and Volcano plots were created in Perseus to identify protein regulations. Upon hypoxia, OVCAR-3 cells show noticeably more regulated proteins, both in CYT and NE, than SKOV-3, whereas upon shear stress, considerably more regulations are evident in SKOV-3 cells. Hardly any identically regulated proteins were observed for both cell lines, except for the NE of the shear stress experiments, with 48 common regulated proteins detected (compare Fig. 9).

4.2.1. Proteome Profiling

SKOV-3 cells stimulated for 24 h with hypoxic exposure showed a total of only 22 protein regulations, with 12 cytoplasmic and 10 nuclear proteins significantly regulated. As evident from the PCAs, the samples could clearly be separated with respect to their different oxygen treatments.

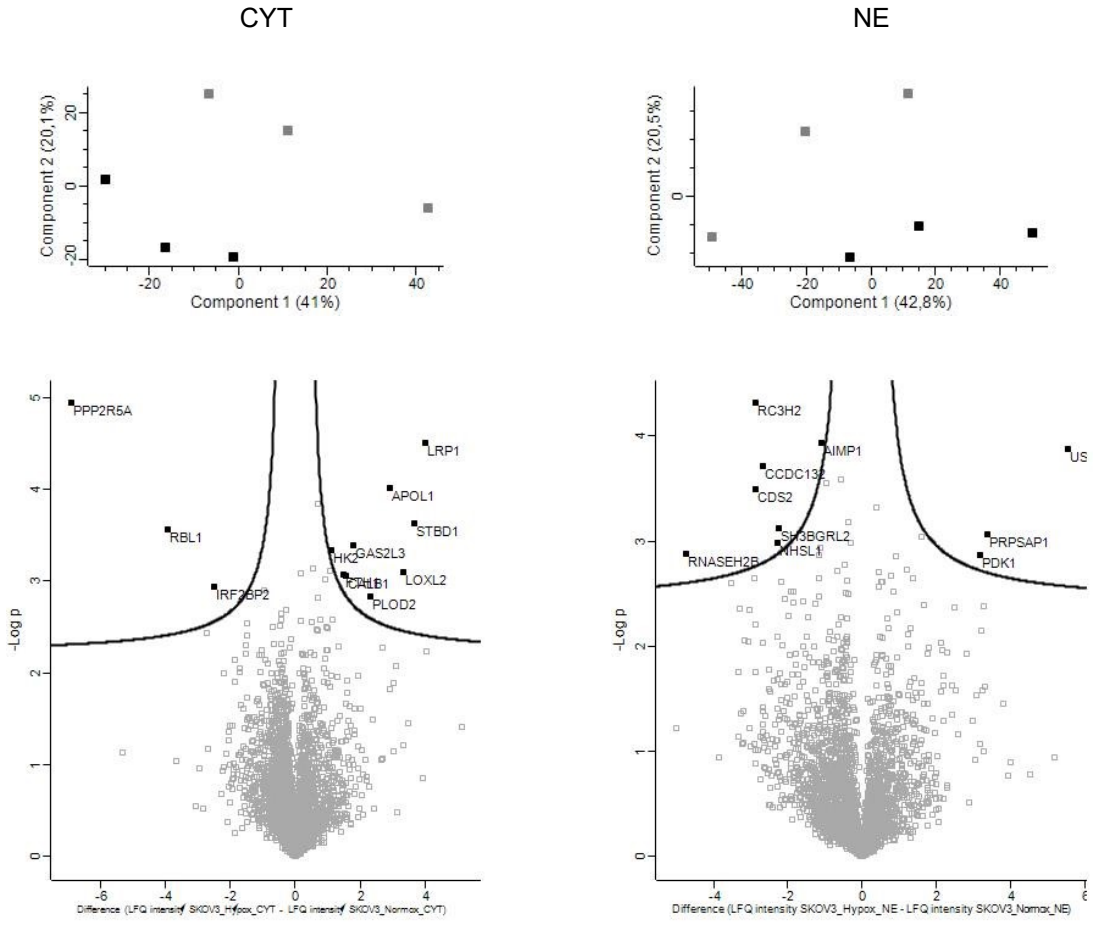

Figure 15 Principal component analyses (top) of SKOV-3 cells after 24 h hypoxic treatment for cytoplasmic (CYT, left) and nuclear (NE, right) fraction. Volcano plots (bottom) of SKOV-3 cells after 24 h hypoxic treatment for cytoplasmic (CYT, left) and nuclear (NE, right) fraction. Hypoxic condition at 1% O_2. Normoxic control (grey), hypoxia (black). FDR < 0.05, S0 = 0.1. Note: Gene names of significantly regulated proteins are indicated according to UniProt database.

Upon shear stress, SKOV-3 cells showed quite more protein regulations, namely 699, with 196 cytoplasmic and 503 nuclear proteins being significantly regulated. The separation of the samples according to their respective biomechanical stimulation (static vs. shear stress) is not flawlessly feasible herein as evident in the PCAs.

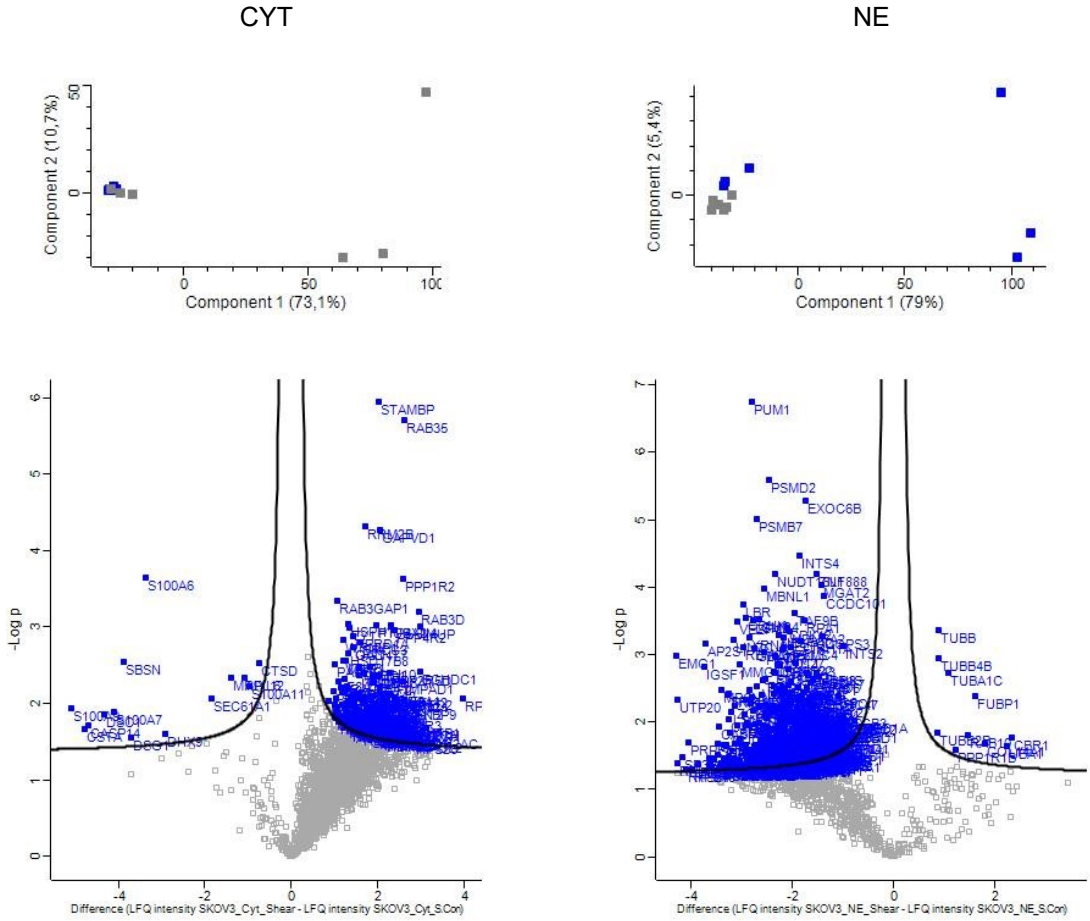

Figure 16 Principal component analyses (top) of SKOV-3 cells after 24 h shear stress treatment for cytoplasmic (CYT, left) and nuclear (NE, right) fraction. Volcano plots (bottom) of SKOV-3 cells after 24 h shear stress treatment for cytoplasmic (CYT, left) and nuclear (NE, right) fraction. Shear stress of 2.8 dyne/cm^2. Static control (grey), shear stress (blue). FDR < 0.05, S0 = 0.1. Note: Gene names of significantly regulated proteins are indicated according to UniProt database.

Three proteins have been found to be significantly regulated in SKOV-3 cells under both conditions, two of them being found in the cytoplasmic (PLOD2 and HK2) fraction and one in the nuclear fraction, namely AIMP1. Both cytoplasmic proteins, PLOD2 and HK2, are upregulated under hypoxia as well as under shear stress. AIMP1 is under both conditions downregulated, and in OVCAR-3 cells in the nuclear fraction of biomechanically stimulated cells.

PLOD2 and HK2, by the way, are the two cytoplasmic proteins which are upregulated in both SKOV-3 and OVCAR-3 under hypoxia (see Fig. 9).

OVCAR-3 cells incubated for 24 h under hypoxia revealed with 138 (38 cytoplasmic and 100 nuclear proteins) notably more regulated proteins than SKOV-3. PCAs show a clear separation of the samples upon their oxygen exposure.

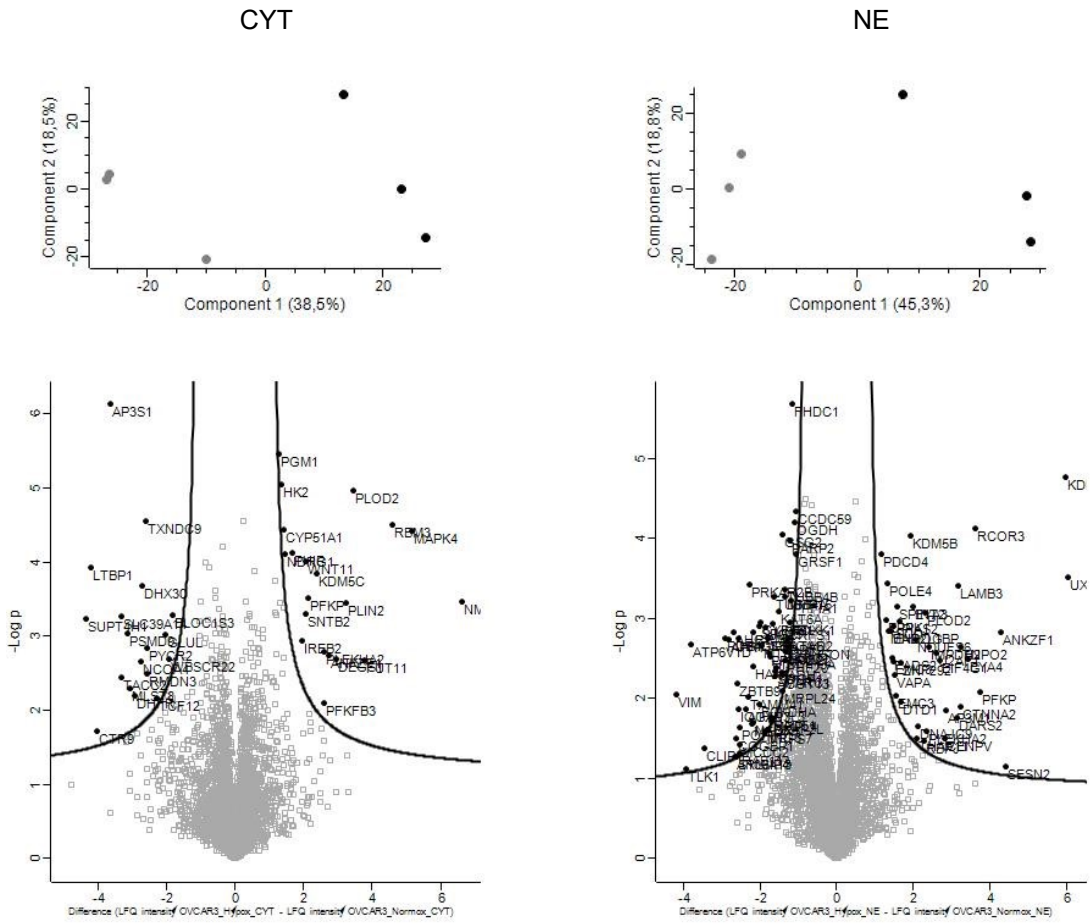

Figure 17 Principal component analyses (top) of OVCAR-3 cells after 24 h hypoxic treatment for cytoplasmic (CYT, left) and nuclear (NE, right) fraction. Volcano plots (bottom) of OVCAR-3 cells after 24 h hypoxic treatment for cytoplasmic (CYT, left) and nuclear (NE, right) fraction. Hypoxic condition at 1% O_2. Normoxic control (grey), hypoxia (black). FDR < 0.05, S0 = 0.5. Note: Gene names of significantly regulated proteins are indicated according to UniProt database.

Shear stress induced quite a few regulations in OVCAR-3 cells with a total of 189 significantly regulated proteins. 16 cytoplasmic and 173 nuclear proteins were determined. The PCAs show a somewhat acceptable separation of the samples with respect to their biomechanical treatments.

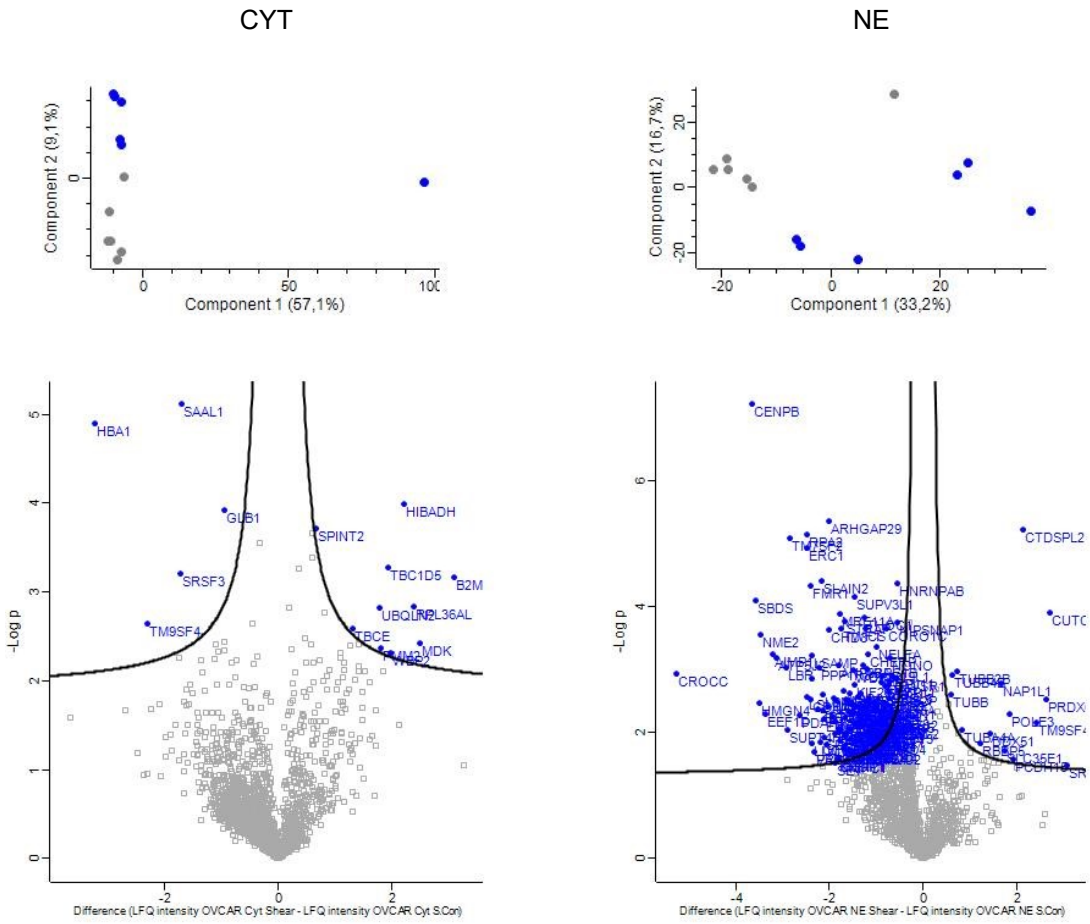

Figure 18 Principal component analyses (top) of OVCAR-3 cells after 24 h shear stress treatment for cytoplasmic (CYT, left) and nuclear (NE, right) fraction. Volcano plots (bottom) of OVCAR-3 cells after 24 h shear stress treatment for cytoplasmic (CYT, left) and nuclear (NE, right) fraction. Shear stress of 2.8 dyne/cm^2. Static control (grey), shear stress (blue). FDR < 0.05, S0 = 0.1. Note: Gene names of significantly regulated proteins are indicated according to UniProt database.

In OVCAR-3 cells, four proteins were determined to be significantly regulated in both conditions, namely SUPT4H1, NDUFS6, SPINT2, and TUBB4B. Although only two of them (NDUFS6 and TUBB4B) are regulated in the nuclear fraction under both conditions, and the other two in different fractions each. In the nuclear fraction of shear stress treated samples are further tubulin proteins regulated (e.g., TUBA4A), whereby all of them are significantly upregulated, and in the hypoxia samples the tubulin proteins are downregulated. The NDUFS6 protein, on the other hand, is upregulated under hypoxia but upon shear stress downregulated. SPINT2 is in both conditions upregulated, and SUPT4H1 downregulated. Regarding the one cytoplasmic protein regulated by both cell lines under shear stress, it is SPINT2. Among the 48 nuclear proteins regulated in both cell lines are NDUFS6, SUPT4H1, and various tubulins, such as TUBB4B.

4.2.2. Phospho Profiling

After 3 h incubation, SKOV-3 cells show no significant regulations for hypoxia, and only two proteins for shear stress. Separation of the samples according to their incubations is rather difficult, but decently visible in the PCA.

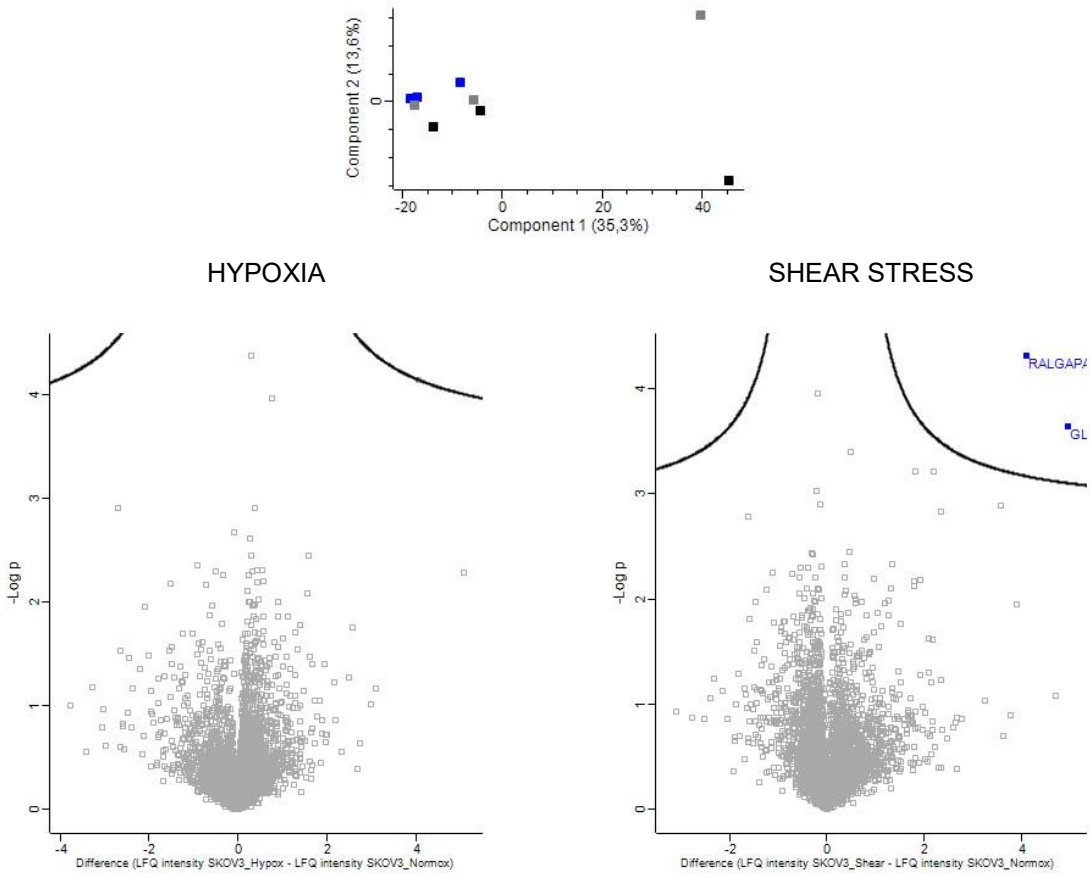

Figure 19 Principal component analysis (top) of whole cell lysis of SKOV-3 cells after 3 h treatments. Volcano plots (bottom) of whole cell lysis of SKOV-3 cells after 3 h treatments. Normoxic static control (grey), hypoxic condition at 1% O_2 (hypoxia, black), shear stress of 2.8 dyne/cm^2 (shear stress, blue). FDR < 0.05, S0 = 0.1. Note: Gene names of significantly regulated proteins are indicated according to UniProt database.

OVCAR-3 cells also show after 3 h incubation no regulations for hypoxia, but for shear stress, namely nine proteins. PCA showing rather poor separation of the samples between hypoxia and normoxic static control, whereas shear stress sample is quite well separated.

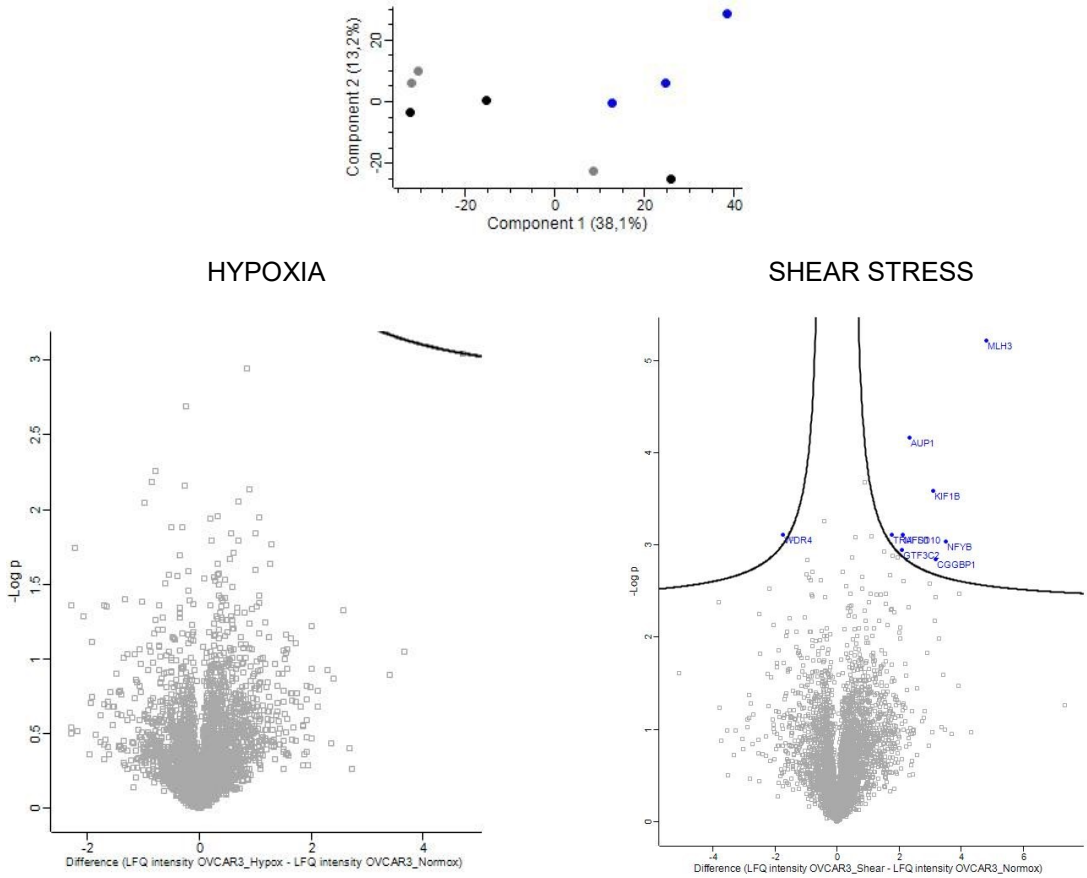

Figure 20 Principal component analysis (top) of whole cell lysis of OVCAR-3 cells after 3 h treatments. Volcano plots (bottom) of whole cell lysis of OVCAR-3 cells after 3 h treatments. Normoxic static control (grey), hypoxic condition at 1% O_2 (hypoxia, black), shear stress of 2.8 dyne/cm^2 (shear stress, blue). FDR < 0.05, S0 = 0.1. Note: Gene names of significantly regulated proteins are indicated according to UniProt database.

5. Discussion and Conclusion

OC is a malignancy with fatal outcome due to commonly very vague symptoms resulting in late diagnosis. A progressed OC has typically already metastasized and spread throughout the peritoneal cavity, so that the cancer cells are exposed to several physical and chemical cues. This microenvironment of biomechanical stimuli and chemical factors, creating ideal conditions for tumor progression, may contribute significantly to drug resistance of advanced stage OC. This thesis investigated morphological and (phospho-)proteomic alterations of two distinct ovarian adenocarcinoma cell lines, SKOV-3 (non-miliary) and OVCAR-3 (miliary), regarding hypoxia and shear stress.

The original idea was to always cultivate both cell lines in each plate (top three wells SKOV-3, and bottom three wells OVCAR-3, for example), but this was not feasible for the subsequent proteomic analyses due to too long preparation times for adjusting zoom and focus on the microscope. To obtain comparable and hence evaluable images, it is advantageous to acquire all images of each condition (here hypoxic, normoxic/static control, and shear stress) with the same microscope, which in this case was the Lionheart™ FX Automated Microscope. While designing the experimental setup, it became clear that it would be better to keep only one cell line per plate to avoid excessive time delays in the imaging of a plate due to zooming and focusing times among the cell lines and thus to ensure a more rapid workflow, which is particularly imperative for the experimental procedure of the phospho-proteomic experiments but is also of great importance for the untargeted proteome analyses. For the cell disruption (lysis) after each incubation in the respective condition, for both 3 and 24 h, it was crucial to work quickly and accurately and to not lose any time during image acquisition, but also to achieve a given image quality to obtain representative and reliable ultrastructural results based on the image analyses. Consequently, to be able to acquire all images of the respective conditions before and after the corresponding incubation time with the Lionheart™ FX Automated Microscope and simultaneously not to reach too long acquisition times, we decided within the scope of the experimental setup to only cultivate and examine one cell line per plate for each experimental run, i.e., not both cell lines per plate (top SKOV-3, bottom OVCAR-3), as originally intended.

Even though both cell lines proliferated well under both experimental conditions (hypoxia and shear stress), the cell number of OVCAR-3 cells was visibly smaller compared to the respective controls after 24 h of treatment, i.e., instead of doubling (see cell counts of normoxic/static control), OVCAR-3 cells proliferated only by around the half within 24 hours under hypoxia as well as under shear stress. Moreover, OVCAR-3 cells exhibited significant changes in size and shape after already 3 h of incubation under hypoxia or shear stress, and in addition, obvious differences in the morphology of hypoxic cells in comparison with normoxic cells. Interestingly, no significant regulated proteins were determined for hypoxia samples but for shear stress after 3 h incubation, namely nine proteins. SKOV-3 cells, however, showed no visible differences between the different treatments, but equally significant changes in morphology after 3 h compared to before. Based on the approximately equal changes in morphology after 3 h in comparison to prior the incubation, it can be suggested that SKOV-3 cells overall were not affected to the extent that they appeared to proliferate normally.

A more detailed look at the phase contrast images reveals that OVCAR-3 cells principally grow in clusters, and when incubated for 24 h under biomechanical stimulation, namely fluid shear stress, they visibly relax and grow more broadly than the corresponding static control (see Fig. 12 top). By contrast, SKOV-3 cells grow in a regular pattern of cells and relax under induced hypoxia (compare Fig. 10 top). Thus, it could be concluded that the miliary OC cells (OVCAR-3) are at their best in shear stress, whereas the non-miliary OC cells (SKOV-3) are the most comfortable under hypoxia.

Since both cell lines visibly increased their size and thus their surface area under hypoxia compared with the normoxic control (Fig. 10 and 12 bottom), it can be assumed that cells in hypoxia increase their surface area to take up more oxygen. This would be consistent with the published data of Zhang *et al.* 2014 [113] and Rohnalter *et al.* 2015 [114], as both reported the induction of giant SKOV-3 cells under hypoxia.

The increase in nuclei areas for both cell lines upon hypoxia, as determined by the fluorescence analyses performed with Gen5 software (see section 3.1.3. Live cell imaging and image analysis), agrees with the increase in cell size determined by morphological analysis. Presumably, an increase in nuclear area is equally due to the reduced oxygen level of 1% in the experimental environment and is part of the generation of hypoxia-induced giant cells. [113, 114] Absence of increase in the mean mitochondrial area of SKOV-3 cells subjected to hypoxia (compared to normoxic control cells and to OVCAR-3 cells too, which showed an increase under both hypoxic and control conditions) indicates that mitochondria in SKOV-3 cells suffer from oxygen deprivation, as supported by the decrease in the mean integrated Mito fluorescence upon hypoxia, as fluorescence increased under normal oxygen condition. For OVCAR-3 cells, on the other hand, the integrated Mito fluorescence is quite stable upon normoxia and increases under reduced oxygen. These contrary results of the fluorescence data of mitochondria obtained from the two cell lines can probably be attributed to the different types (miliary vs. non-miliary) of ovarian carcinoma. [115]

Yamamoto et al. 2018 described shear stress induced mitochondrial ATP generation, which might be activated by a caveolae or CAV1 dependent mechanism. The transfer of caveolins, such as CAV1, between caveolae and mitochondria is thought to be of great importance, especially in dealing with cellular stress, like shear stress. A lack of CAV1, whether hypoxia or shear stress induced, affects mitochondrial functions by cholesterol accumulation, leading to decreased efficiency of the respiratory chain. [116] The evaluated fluorescence data of shear stress experiments within this thesis show for both Mito area and integrated Mito fluorescence little changes over the 24 h of treatment, whereas for both cell lines a visible increase under static control condition was determined, indicating that the exposure to biomechanical stimulation affects the intensity of mitochondria signal.

When comparing the cell lines, more protein regulations for OVCAR-3 cells are revealed after 24 h of hypoxia, and more regulations for SKOV-3 cells after 24 h shear stress treatment (compare Fig. 9), thus it can be assumed that SKOV-3 cells are more sensitive towards biomechanical stimulation, whereas OVCAR-3 cells are more responsive to reduced oxygen. This in turn implies that the cell line representing the miliary type (OVCAR-3) answers with more protein regulations to hypoxic exposure, and the cell line serving as model for the non-miliary type (SKOV-3) is more responsive to the artificial

fluid shear stress. This fits with the above-mentioned finding of the morphological analyses, that OVCAR-3 seem to be more comfortable under shear stress and SKOV-3 under hypoxia. Comparing this with the assumed origin of both types, it makes sense, as they are acclimated to the respective conditions that are supposed to mimic the corresponding TME. Miliary OC cells are thought to be well accustomed to fluid shear stress, as they are widespread, millet-sized lesions, and thus are not particularly affected by fluid shear stress during the experimental procedure. Non-miliary OC cells, on the other hand, are usually found in larger, excessively growing tumor implants. [27, 115]

The signaling pathways mentioned in section 1.1., such as MAPK and PI3K, and the mutations or respectively the overexpression of genes (BRAF, KRAS, and p53) associated with the different types (I and II) of OC are equally important in the development of the generally less malignant borderline ovarian tumors. [117] So in turn it can be assumed that these signaling pathways are not only disrupted among aggressive malignant OCs, but an impairment is typical when it comes to any cellular abnormalities.

Hypoxia is well known to be associated with several signaling pathways involved in various cellular processes such as proliferation, apoptosis, or metabolism, prominent among them PI3K, MAPK, or NFκB. [118-123] In addition, hypoxia contributes to resistance against treatments, i.e., the adaption processes are controlled by hypoxia by activating the above-mentioned signaling pathways. Nevertheless, these signaling pathways can also be activated regardless of hypoxia. [36] Johnson *et al.* 2011 described that shear stress obviously activates several signal transduction pathways, including the previously mentioned PI3K, MAPK, and NFκB pathways, but also the focal adhesion kinase (FAK), Rho family guanosine triphosphate (GTP)-ases, and protein kinase C (PKC) signaling pathways. [124]

In accordance with literature, we identified several proteins as significantly regulated, such as PLOD2, which was upregulated in both cell lines under hypoxia and in SKOV-3 cells also under shear stress, and various MAP kinases, or the mesenchymal marker Vimentin, which was determined to be significantly downregulated in the nuclear extract of hypoxic OVCAR-3 cells, whereas according to literature, Vimentin is upregulated by hypoxia in human ovarian cell lines (i.e., SKOV-3 cells). [29] A final extensive molecular interpretation and discussion as well as a breakdown of the proteomics data (pathway analysis) is beyond the scope of this master's thesis and can be found in Bileck *et al*. which is currently submitted for publication. All the mentioned signaling pathways, which are impaired according to literature, illustrate why phosphorylation events have been investigated within this thesis and why they provide valuable information about cellular processes.

As previously mentioned, neither cell line showed significant protein regulations after 3 h incubation under hypoxia, but for shear stress samples, regulations for both SKOV-3 (two proteins) and OVCAR-3 (nine proteins) were found. Nonetheless, it should be noted that the basic proteome of both cell lines remained almost unchanged after 3 h of treatment (hypoxia as well as shear stress), which is also visible in the respective PCAs, as for both cell lines only decent separations are evident according to their treatments. The Analysis of the phospho-proteome (after phosphopeptide enrichment) revealed a couple of regulations, which were not shown nor discussed in this master's thesis. Detailed description and discussion of the phospho-proteome results are also provided in Bileck *et al.* currently submitted for publication.

Within this thesis, the experimental design proved capable of adequately mimicking the ovarian cancer microenvironment and thus performing experiments more accurate to the *in vivo* situation. Potential future experimental designs could consider simultaneous hypoxic and shear stress, although this would need to be implemented with different methodology and/or equipment. In addition, chemotaxis and 3D culture could also be considered in the experimental setup. On top, the experiments could be performed with cocultures of ovarian cancer, stromal, and immune cells to simulate the *in vivo* situation of the peritoneal cavity more accurately, as previously mentioned in Novak *et al.* 2018. [44]

In the scope of this thesis, significant morphological as well as proteomic differences were revealed for both treatments, thus underlining that conventional cell culture experimentations (i.e., without any biomechanical movement or chemical stimulation, which would be usual for the respective TME) tend to be too unreliable with respect to the *in vivo* situations. For better investigation of potential anticancer drugs intended for OC, *in vitro* studies evaluating these drugs need to be performed under hypoxic or shear stress conditions, ideally under combined treatment.

References

1. Nash, Z. and U. Menon, *Ovarian cancer screening: Current status and future directions.* Best Practice & Research Clinical Obstetrics & Gynaecology, 2020. **65**: p. 32-45.
2. Stewart, C., C. Ralyea, and S. Lockwood, *Ovarian Cancer: An Integrated Review.* Seminars in Oncology Nursing, 2019. **35**(2): p. 151-156.
3. Momenimovahed, Z., et al., *Ovarian cancer in the world: epidemiology and risk factors.* International Journal of Women's Health, 2019. **Volume 11**: p. 287-299.
4. Prat, J. and D.G. Mutch, *Pathology of cancers of the female genital tract including molecular pathology.* International Journal of Gynecology & Obstetrics, 2018. **143**: p. 93-108.
5. Michelle A. Roett, M., MPH, and Patricia Evans, MD, *Ovarian Cancer: An Overview.* American Family Physician, 2009. **80**.
6. Budiana, I.N.G., M. Angelina, and T.G.A. Pemayun, *Ovarian cancer: Pathogenesis and current recommendations for prophylactic surgery.* Journal of the Turkish-German Gynecological Association, 2019. **20**(1): p. 47-54.
7. Kurman, R.J. and I.-M. Shih, *The Origin and Pathogenesis of Epithelial Ovarian Cancer: A Proposed Unifying Theory.* American Journal of Surgical Pathology, 2010. **34**(3): p. 433-443.
8. Erickson, B.K., M.G. Conner, and C.N. Landen, *The role of the fallopian tube in the origin of ovarian cancer.* American Journal of Obstetrics and Gynecology, 2013. **209**(5): p. 409-414.
9. Koshiyama, M., N. Matsumura, and I. Konishi, *Recent Concepts of Ovarian Carcinogenesis: Type I and Type II.* BioMed Research International, 2014. **2014**: p. 1-11.
10. Bekos, C., et al., *NECTIN4 (PVRL4) as Putative Therapeutic Target for a Specific Subtype of High Grade Serous Ovarian Cancer-An Integrative Multi-Omics Approach.* Cancers (Basel), 2019. **11**(5).
11. Muqaku, B., et al., *Neutrophil Extracellular Trap Formation Correlates with Favorable Overall Survival in High Grade Ovarian Cancer.* Cancers (Basel), 2020. **12**(2).
12. Auer, K., et al., *Comparative transcriptome analysis links distinct peritoneal tumor spread types, miliary and non-miliary, with putative origin, tubes and ovaries, in high grade serous ovarian cancer.* Cancer Lett, 2017. **388**: p. 158-166.
13. Huang, C.-Y., et al., *Comparing Paclitaxel–Carboplatin with Paclitaxel–Cisplatin as the Front-Line Chemotherapy for Patients with FIGO IIIC Serous-Type Tubo-Ovarian Cancer.* International Journal of Environmental Research and Public Health, 2020. **17**(7): p. 2213.
14. Boussios, S., et al., *Poly (ADP-Ribose) Polymerase Inhibitors: Talazoparib in Ovarian Cancer and Beyond.* Drugs in R&D, 2020.
15. Sehouli, J. and J.P. Grabowski, *Surgery in recurrent ovarian cancer.* Cancer, 2019. **125**(S24): p. 4598-4601.
16. Bachmayr-Heyda, A., et al., *Integrative Systemic and Local Metabolomics with Impact on Survival in High-Grade Serous Ovarian Cancer.* Clin Cancer Res, 2017. **23**(8): p. 2081-2092.
17. De, A., et al., *Sensitization of Carboplatinum- and Taxol-Resistant High-Grade Serous Ovarian Cancer Cells Carrying p53, BRCA1/2 Mutations by Emblica officinalis (Amla) via Multiple Targets.* J Cancer, 2020. **11**(7): p. 1927-1939.
18. Del Carmen, M.G., et al., *Synergism of Epidermal Growth Factor Receptor–Targeted Immunotherapy With Photodynamic Treatment of Ovarian Cancer In Vivo.* JNCI: Journal of the National Cancer Institute, 2005. **97**(20): p. 1516-1524.
19. Fowers, K.D. and J. Kopeček, *Targeting of Multidrug-Resistant Human Ovarian Carcinoma Cells With Anti-P-Glycoprotein Antibody Conjugates.* Macromolecular Bioscience, 2012. **12**(4): p. 502-514.
20. Xie, W., et al., *miR-197-3p reduces epithelial–mesenchymal transition by targeting ABCA7 in ovarian cancer cells.* 3 Biotech, 2020. **10**(8).

21. Nunes, S.C., et al., *Cysteine allows ovarian cancer cells to adapt to hypoxia and to escape from carboplatin cytotoxicity.* Sci Rep, 2018. **8**(1): p. 9513.

22. Feng, L., et al., *Hypoxia-induced up-regulation of miR-27a promotes paclitaxel resistance in ovarian cancer.* Bioscience Reports, 2020. **40**(4).

23. Nath, S., et al., *Flow-induced Shear Stress Confers Resistance to Carboplatin in an Adherent Three-Dimensional Model for Ovarian Cancer: A Role for EGFR-Targeted Photoimmunotherapy Informed by Physical Stress.* J Clin Med, 2020. **9**(4).

24. Nunes, S.C., et al., *Cysteine boosters the evolutionary adaptation to CoCl2 mimicked hypoxia conditions, favouring carboplatin resistance in ovarian cancer.* BMC Evol Biol, 2018. **18**(1): p. 97.

25. Zhang, H., et al., *Hypoxia-Inducible Factor-1alpha (HIF-1alpha) Promotes Hypoxia-Induced Invasion and Metastasis in Ovarian Cancer by Targeting Matrix Metallopeptidase 13 (MMP13).* Med Sci Monit, 2019. **25**: p. 7202-7208.

26. Gómez-Raposo, C., et al., *Angiogenesis and ovarian cancer.* Clinical and Translational Oncology, 2009. **11**(9): p. 564-571.

27. Auer, K., et al., *Role of the immune system in the peritoneal tumor spread of high grade serous ovarian cancer.* Oncotarget, 2016. **7**: p. 61336-61354.

28. Dovnik, A. and N. Fokter Dovnik, *Vitamin D and Ovarian Cancer: Systematic Review of the Literature with a Focus on Molecular Mechanisms.* Cells, 2020. **9**(2): p. 335.

29. Qin, J., et al., *Hypoxia-inducible factor 1 alpha promotes cancer stem cells-like properties in human ovarian cancer cells by upregulating SIRT1 expression.* Sci Rep, 2017. **7**(1): p. 10592.

30. McEvoy, L.M., et al., *Identifying novel hypoxia-associated markers of chemoresistance in ovarian cancer.* BMC Cancer, 2015. **15**: p. 547.

31. Yue, P., et al., *Hyperactive EGF receptor, Jaks and Stat3 signaling promote enhanced colony-forming ability, motility and migration of cisplatin-resistant ovarian cancer cells.* Oncogene, 2012. **31**(18): p. 2309-2322.

32. Natarajan, S., et al., *Collagen Remodeling in the Hypoxic Tumor-Mesothelial Niche Promotes Ovarian Cancer Metastasis.* Cancer Res, 2019. **79**(9): p. 2271-2284.

33. Campioni, M., et al., *Role of Apaf-1, a key regulator of apoptosis, in melanoma progression and chemoresistance.* Experimental Dermatology, 2005. **14**(11): p. 811-818.

34. Au Yeung, C.L., et al., *Exosomal transfer of stroma-derived miR21 confers paclitaxel resistance in ovarian cancer cells through targeting APAF1.* Nature Communications, 2016. **7**(1): p. 11150.

35. Li, J., et al., *Overexpression of miRNA-221 promotes cell proliferation by targeting the apoptotic protease activating factor-1 and indicates a poor prognosis in ovarian cancer.* International Journal of Oncology, 2017. **50**(4): p. 1087-1096.

36. Muz, B., et al., *The role of hypoxia in cancer progression, angiogenesis, metastasis, and resistance to therapy.* Hypoxia, 2015: p. 83.

37. Sakata, K., et al., *Hypoxia-induced drug resistance: comparison to P-glycoprotein-associated drug resistance.* British Journal of Cancer, 1991. **64**(5): p. 809-814.

38. Kato, Y., et al., *Effects of Acute and Chronic Hypoxia on the Radiosensitivity of Gastric and Esophageal Cancer Cells.* Anticancer Res, 2011. **31**: p. 3369-3376.

39. Edin, N.J., et al., *Low dose hyper-radiosensitivity is eliminated during exposure to cycling hypoxia but returns after reoxygenation.* Int J Radiat Biol, 2012. **88**(4): p. 311-9.

40. Zanotelli, M.R. and C.A. Reinhart-King, *Mechanical Forces in Tumor Angiogenesis*. 2018, Springer International Publishing. p. 91-112.

41. Capobianco, A., et al., *The peritoneum: healing, immunity, and diseases.* The Journal of Pathology, 2017. **243**(2): p. 137-147.

42. Ip, C.K.M., et al., *Stemness and chemoresistance in epithelial ovarian carcinoma cells under shear stress.* Scientific Reports, 2016. **6**(1): p. 26788.

43. Carmignani, C.P., et al., *Intraperitoneal cancer dissemination: Mechanisms of the patterns of spread.* Cancer and Metastasis Reviews, 2003. **22**(4): p. 465-472.

44. Novak, C., E. Horst, and G. Mehta, *Review: Mechanotransduction in ovarian cancer: Shearing into the unknown.* APL Bioengineering, 2018. **2**(3): p. 031701.

45. Rizvi, I., et al., *Flow induces epithelial-mesenchymal transition, cellular heterogeneity and biomarker modulation in 3D ovarian cancer nodules.* Proceedings of the National Academy of Sciences, 2013. **110**(22): p. E1974-E1983.

46. Lengyel, E., *Ovarian Cancer Development and Metastasis.* The American Journal of Pathology, 2010. **177**(3): p. 1053-1064.

47. Wilkins, M., *Proteomics Data Mining.* Expert Review of Proteomics, 2009. **6**(6): p. 599-603.

48. Timp, W. and G. Timp, *Beyond mass spectrometry, the next step in proteomics.* Science Advances, 2020. **6**(2): p. eaax8978.

49. Beynon, R.J., *The dynamics of the proteome: Strategies for measuring protein turnover on a proteome-wide scale.* Briefings in Functional Genomics and Proteomics, 2005. **3**(4): p. 382-390.

50. Graves, P.R. and T.A.J. Haystead, *Molecular Biologist's Guide to Proteomics.* Microbiology and Molecular Biology Reviews, 2002. **66**(1): p. 39-63.

51. Twyman, R.M., *Proteomics*. 2012, Elsevier. p. 642-649.

52. O'Farrell, P., *High resolution two-dimensional electrophoresis of proteins.* Journal of Biological Chemistry, 1975. **250**(10): p. 4007-4021.

53. Klose, J., *Protein Mapping by Combined Isoelectric Focusing and Electrophoresis of Mouse Tissues.* Humangenetik, 1975. **26**: p. 231-243.

54. Scheele, G.A., *Two-dimensional gel analysis of soluble proteins. Charaterization of guinea pig exocrine pancreatic proteins.* Journal of Biological Chemistry, 1975. **250**(14): p. 5375-5385.

55. Anderson, N.L. and N.G. Anderson, *Proteome and proteomics: New technologies, new concepts, and new words.* Electrophoresis, 1998. **19**(11): p. 1853-1861.

56. Edman, P., *A method for the determination of amino acid sequence in peptides.* Arch Biochem, 1949. **22**(3): p. 475.

57. Patterson, S.D. and R.H. Aebersold, *Proteomics: the first decade and beyond.* Nature Genetics, 2003. **33**(S3): p. 311-323.

58. Andersen, J.S. and M. Mann, *Functional genomics by mass spectrometry.* FEBS Letters, 2000. **480**(1): p. 25-31.

59. Bekker-Jensen, D.B., et al., *A Compact Quadrupole-Orbitrap Mass Spectrometer with FAIMS Interface Improves Proteome Coverage in Short LC Gradients.* Mol Cell Proteomics, 2020. **19**(4): p. 716-729.

60. Blackstock, W.P. and M.P. Weir, *Proteomics: quantitative and physical mapping of cellular proteins.* Trends in Biotechnology, 1999. **17**(3): p. 121-127.

61. Wilson, D.H., et al., *The Simoa HD-1 Analyzer.* Journal of Laboratory Automation, 2016. **21**(4): p. 533-547.

62. Manadas, B., et al., *Peptide fractionation in proteomics approaches.* Expert Review of Proteomics, 2010. **7**(5): p. 655-663.

63. Weston, A.D. and L. Hood, *Systems Biology, Proteomics, and the Future of Health Care: Toward Predictive, Preventative, and Personalized Medicine.* Journal of Proteome Research, 2004. **3**(2): p. 179-196.

64. Aebersold, R. and M. Mann, *Mass spectrometry-based proteomics.* Nature, 2003. **422**(6928): p. 198-207.

65. Resing, K.A. and N.G. Ahn, *Proteomics strategies for protein identification.* FEBS Letters, 2005. **579**(4): p. 885-889.

66. Fournier, M.L., et al., *Multidimensional Separations-Based Shotgun Proteomics.* Chemical Reviews, 2007. **107**(8): p. 3654-3686.

67. Nesvizhskii, A.I., *Protein identification by tandem mass spectrometry and sequence database searching.* Methods Mol Biol, 2007. **367**: p. 87-119.

68. Griss, J., et al., *Recognizing millions of consistently unidentified spectra across hundreds of shotgun proteomics datasets.* Nature Methods, 2016. **13**(8): p. 651-656.

69. Cohen, P., *The origins of protein phosphorylation.* Nature Cell Biology, 2002. **4**(5): p. E127-E130.

70. Vlastaridis, P., et al., *Estimating the total number of phosphoproteins and phosphorylation sites in eukaryotic proteomes.* GigaScience, 2017. **6**(2): p. 1-11.

71. Singh, V., et al., *Phosphorylation: Implications in Cancer.* The Protein Journal, 2017. **36**(1): p. 1-6.

72. Needham, E.J., et al., *Illuminating the dark phosphoproteome.* Science Signaling, 2019. **12**(565): p. eaau8645.

73. Bateman, A., et al., *UniProt: the universal protein knowledgebase in 2021.* Nucleic Acids Research, 2021. **49**(D1): p. D480-D489.

74. Hornbeck, P.V., et al., *PhosphoSite: A bioinformatics resource dedicated to physiological protein phosphorylation.* PROTEOMICS, 2004. **4**(6): p. 1551-1561.

75. Gnad, F., J. Gunawardena, and M. Mann, *PHOSIDA 2011: the posttranslational modification database.* Nucleic Acids Research, 2011. **39**(Database): p. D253-D260.

76. Minguez, P., et al., *Deciphering a global network of functionally associated post-translational modifications.* Molecular Systems Biology, 2012. **8**(1): p. 599.

77. Ardito, F., et al., *The crucial role of protein phosphorylation in cell signaling and its use as targeted therapy (Review).* International Journal of Molecular Medicine, 2017. **40**(2): p. 271-280.

78. Fruman, D.A., et al., *The PI3K Pathway in Human Disease.* Cell, 2017. **170**(4): p. 605-635.

79. Hornbeck, P.V., et al., *PhosphoSitePlus, 2014: mutations, PTMs and recalibrations.* Nucleic Acids Research, 2015. **43**(D1): p. D512-D520.

80. Solari, F.A., et al., *Why phosphoproteomics is still a challenge.* Molecular BioSystems, 2015. **11**(6): p. 1487-1493.

81. Dickhut, C., et al., *Impact of Digestion Conditions on Phosphoproteomics.* 2014. **13**(6): p. 2761-2770.

82. Humphrey, S.J., et al., *High-throughput and high-sensitivity phosphoproteomics with the EasyPhos platform.* Nature Protocols, 2018. **13**(9): p. 1897-1916.

83. de Graaf, E.L., et al., *Single-step enrichment by Ti4+-IMAC and label-free quantitation enables in-depth monitoring of phosphorylation dynamics with high reproducibility and temporal resolution.* Mol Cell Proteomics, 2014. **13**(9): p. 2426-34.

84. Li, X.-S., B.-F. Yuan, and Y.-Q. Feng, *Recent advances in phosphopeptide enrichment: Strategies and techniques.* TrAC Trends in Analytical Chemistry, 2016. **78**: p. 70-83.

85. Thingholm, T.E., et al., *TiO 2 -Based Phosphoproteomic Analysis of the Plasma Membrane and the Effects of Phosphatase Inhibitor Treatment.* 2008. **7**(8): p. 3304-3313.

86. Hogrebe, A., et al., *Benchmarking common quantification strategies for large-scale phosphoproteomics.* Nature Communications, 2018. **9**(1).

87. Yates, J.R., 3rd, *Mass spectrometry and the age of the proteome.* J Mass Spectrom, 1998. **33**(1): p. 1-19.

88. Griffiths, J., *A Brief History of Mass Spectrometry.* Analytical Chemistry, 2008. **80**(15): p. 5678-5683.

89. Wilkinson, D.J., *Historical and contemporary stable isotope tracer approaches to studying mammalian protein metabolism.* Mass Spectrometry Reviews, 2018. **37**(1): p. 57-80.

90. Barber, M., et al., *Fast atom bombardment of solids (F.A.B.): a new ion source for mass spectrometry.* Journal of the Chemical Society, Chemical Communications, 1981(7): p. 325.

91. James, P., *Protein identification in the post-genome era: the rapid rise of proteomics.* Quarterly Reviews of Biophysics, 1997. **30**(4): p. 279-331.

92. Dole, M., et al., *Molecular Beams of Macroions.* The Journal of Chemical Physics, 1968. **49**(5): p. 2240-2249.

93. Covey, T.R., et al., *The determination of protein, oligonucleotide and peptide molecular weights by ion-spray mass spectrometry.* Rapid Commun Mass Spectrom, 1988. **2**(11): p. 249-56.

94. Fenn, J.B., et al., *Electrospray Ionization for Mass Spectrometry of Large Biomolecules.* Science, 1989. **246**(4926): p. 64-71.

95. Karas, M. and F. Hillenkamp, *Laser desorption ionization of proteins with molecular masses exceeding 10,000 daltons.* Analytical Chemistry, 1988. **60**(20): p. 2299-2301.

96. Ridgeway, M.E., et al., *Trapped ion mobility spectrometry: A short review.* International Journal of Mass Spectrometry, 2018. **425**: p. 22-35.

97. Hörth, P., et al., *Efficient Fractionation and Improved Protein Identification by Peptide OFFGEL Electrophoresis.* Molecular & Cellular Proteomics, 2006. **5**(10): p. 1968-1974.

98. Michalski, A., et al., *Mass spectrometry-based proteomics using Q Exactive, a high-performance benchtop quadrupole Orbitrap mass spectrometer.* Mol Cell Proteomics, 2011. **10**(9): p. M111.011015.

99. Hardman, M. and A.A. Makarov, *Interfacing the Orbitrap Mass Analyzer to an Electrospray Ion Source.* Analytical Chemistry, 2003. **75**(7): p. 1699-1705.

100. Scigelova, M. and A. Makarov, *Orbitrap Mass Analyzer – Overview and Applications in Proteomics.* PROTEOMICS, 2006. **6**(S2): p. 16-21.

101. Makarov, A., *Electrostatic Axially Harmonic Orbital Trapping: A High-Performance Technique of Mass Analysis.* Analytical Chemistry, 2000. **72**(6): p. 1156-1162.

102. Syka, J.E.P., et al., *Novel Linear Quadrupole Ion Trap/FT Mass Spectrometer: Performance Characterization and Use in the Comparative Analysis of Histone H3 Post-translational Modifications.* Journal of Proteome Research, 2004. **3**(3): p. 621-626.

103. Fernandez-Lima, F.A., D.A. Kaplan, and M.A. Park, *Note: Integration of trapped ion mobility spectrometry with mass spectrometry.* Review of Scientific Instruments, 2011. **82**(12): p. 126106.

104. Michalski, A., J. Cox, and M. Mann, *More than 100,000 Detectable Peptide Species Elute in Single Shotgun Proteomics Runs but the Majority is Inaccessible to Data-Dependent LC−MS/MS.* Journal of Proteome Research, 2011. **10**(4): p. 1785-1793.

105. Meier, F., et al., *Parallel Accumulation–Serial Fragmentation (PASEF): Multiplying Sequencing Speed and Sensitivity by Synchronized Scans in a Trapped Ion Mobility Device.* Journal of Proteome Research, 2015. **14**(12): p. 5378-5387.

106. Meier, F., et al., *Online Parallel Accumulation–Serial Fragmentation (PASEF) with a Novel Trapped Ion Mobility Mass Spectrometer.* Molecular & Cellular Proteomics, 2018. **17**(12): p. 2534-2545.

107. Vasilopoulou, C.G., et al., *Trapped ion mobility spectrometry and PASEF enable in-depth lipidomics from minimal sample amounts.* Nature Communications, 2020. **11**(1).

108. Oliver, N.A., B.D. Greenberg, and D.C. Wallace, *Assignment of a polymorphic polypeptide to the human mitochondrial DNA unidentified reading frame 3 gene by a new peptide mapping strategy.* Journal of Biological Chemistry, 1983. **258**(9): p. 5834-5839.

109. *Basic Local Alignment Search Tool*. Available from: https://blast.ncbi.nlm.nih.gov/Blast.cgi.

110. Jassal, B., et al., *The reactome pathway knowledgebase.* Nucleic acids research, 2020. **48**(D1): p. D498-D503.

111. Warboys, C.M., M. Ghim, and P.D. Weinberg, *Understanding mechanobiology in cultured endothelium: A review of the orbital shaker method.* Atherosclerosis, 2019. **285**: p. 170-177.

112. Tyanova, S., et al., *The Perseus computational platform for comprehensive analysis of (prote)omics data.* Nature Methods, 2016. **13**(9): p. 731-740.

113. Zhang, S., et al., *Generation of cancer stem-like cells through the formation of polyploid giant cancer cells.* Oncogene, 2014. **33**(1): p. 116-128.

114. Rohnalter, V., et al., *A multi-stage process including transient polyploidization and EMT precedes the emergence of chemoresistent ovarian carcinoma cells with a dedifferentiated and pro-inflammatory secretory phenotype.* Oncotarget, 2015. **6**(37): p. 40005-40025.

115. Auer, K., et al., *Peritoneal tumor spread in serous ovarian cancer-epithelial mesenchymal status and outcome.* Oncotarget, 2015. **6**(19): p. 17261-17275.

116. Yamamoto, K., H. Imamura, and J. Ando, *Shear stress augments mitochondrial ATP generation that triggers ATP release and Ca2+ signaling in vascular endothelial cells.* American Journal of Physiology-Heart and Circulatory Physiology, 2018. **315**(5): p. H1477-H1485.

117. Sun, Y., J. Xu, and X. Jia, *The Diagnosis, Treatment, Prognosis and Molecular Pathology of Borderline Ovarian Tumors: Current Status and Perspectives.* Cancer Management and Research, 2020. **Volume 12**: p. 3651-3659.

118. Agani, F. and B.H. Jiang, *Oxygen-independent regulation of HIF-1: novel involvement of PI3K/AKT/mTOR pathway in cancer.* Curr Cancer Drug Targets, 2013. **13**(3): p. 245-51.

119. Courtnay, R., et al., *Cancer metabolism and the Warburg effect: the role of HIF-1 and PI3K.* Mol Biol Rep, 2015. **42**(4): p. 841-51.

120. Seta, K.A., et al., *Responding to hypoxia: lessons from a model cell line.* Sci STKE, 2002. **2002**(146): p. re11.

121. Sanchez, A., et al., *p38 MAPK: a mediator of hypoxia-induced cerebrovascular inflammation.* J Alzheimers Dis, 2012. **32**(3): p. 587-97.

122. Minet, E., et al., *ERK activation upon hypoxia: involvement in HIF-1 activation.* FEBS Lett, 2000. **468**(1): p. 53-8.

123. Koong, A.C., E.Y. Chen, and A.J. Giaccia, *Hypoxia causes the activation of nuclear factor kappa B through the phosphorylation of I kappa B alpha on tyrosine residues.* Cancer Res, 1994. **54**(6): p. 1425-30.

124. Johnson, B.D., K.J. Mather, and J.P. Wallace, *Mechanotransduction of shear in the endothelium: Basic studies and clinical implications.* Vascular Medicine, 2011. **16**(5): p. 365-377.

List of figures

List of tables

Supplementary Material

Fluorescence analysis

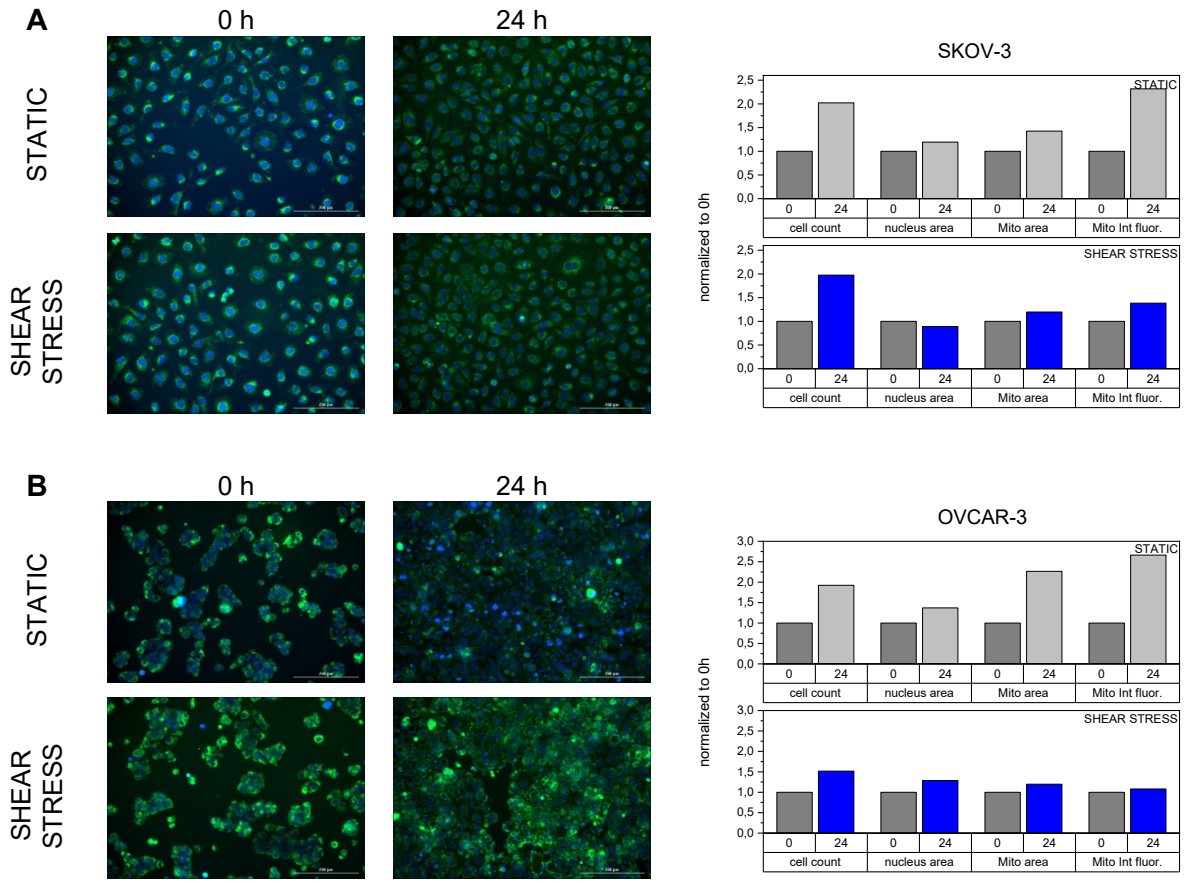

Figure S1 Representative fluorescence images (nuclei in blue, Hoechst, and mitochondria in green, MitoTracker™) of SKOV-3 (A) and OVCAR-3 (B) before and after 24 h shear stress treatment with the corresponding results of fluorescence analyses acquired with Gen5 software. Data are the mean of n = 4 optical fields evaluated for both time points of each treatment per cell line by Gen5 software, no SD calculated.